Accepted Manuscript

Title: Delineating and characterizing the boundary of the Cathaysia Block and the Jiangnan orogenic belt in South China

Author: Jinlong Yao Liangshu Shu Peter A. Cawood Jinyi Li

PII: S0301-9268(16)00032-2
DOI: http://dx.doi.org/doi:10.1016/j.precamres.2016.01.023
Reference: PRECAM 4442

To appear in: *Precambrian Research*

Received date: 4-8-2015
Revised date: 7-1-2016
Accepted date: 11-1-2016

Please cite this article as: Yao, J., Shu, L., Cawood, P.A., Li, J.,Delineating and characterizing the boundary of the Cathaysia Block and the Jiangnan orogenic belt in South China, *Precambrian Research* (2016), http://dx.doi.org/10.1016/j.precamres.2016.01.023

Research highlights

- Ca. 880~850 Ma rock units identified within the Jiangshan-Shaoxing fault zone at Shijiao indicate a convergent plate margin setting
- Field geology and analytical data indicate the Shijiao area display close affinity with Jiangnan belt rather than Cathaysia
- Overall relationships at Shijiao constrain the location of suture between Cathaysia and Jiangnan in NE Zhejiang during Neoproterozoic.

Delineating and characterizing the boundary of the Cathaysia Block and the Jiangnan orogenic belt in South China

Jinlong Yao[a], Liangshu Shu[a,*], Peter A. Cawood[b, c], Jinyi Li[d]

[a] State Key Laboratory for Mineral Deposits Research, School of Earth Sciences and Engineering, Nanjing University, Nanjing 210093, China

[b] Department of Earth Sciences, University of St Andrews, North Street, St Andrews KY16 9AL, UK

[c]School of Earth and Environment, The University of Western Australia, 35 Stirling Highway, Crawley, WA 6009, Australia

[d] Institute of Geology, Chinese Academy of Geological Sciences, Beijing 100037, China

* Corresponding author E–mail: Lsshu@nju.edu.cn

Abstract

The Jiangshan-Shaoxing fault zone lies along the SE margin of the Jiangnan belt, and delineates the northeastern margin of the Cathaysia Block of the South China Craton. At Shijiao in NE Zhejiang, the fault zone consists of hornblende schist intruded by migmatized quartz diorite. It constitutes a shear zone delineating the welded boundary between the Neoproterozoic Shuangxiwu Group of Jiangnan belt to the north and the Chencai Complex of Cathaysia Block to the south. The Shuangxiwu Group is composed mainly of basalt, andesite and flysch, whereas the Chencai

Complex contains magmatic and sedimentary rocks that experienced amphibolite facies metamorphism. Zircons from quartz diorite and gabbro from the fault zone at Shijiao yield ages of 854 ± 6 Ma, 857 ± 5 Ma and 860 ± 5 Ma, with positive εHf(t) values of 7.81~11.8 and 4.57~10.39. The quartz diorite and mafic-ultramafic rock samples display minor LREE enriched pattern with obvious depletion of Nb, Ta, Rb, Ba and Ti, compared to their neighboring elements and plot in the volcanic arc field on geochemical diagrams, similar to that of volcanic rocks from Shuangxiwu Group. Overall relationships within the Jiangshan-Shaoxing fault zone at Shijiao suggest the ca. 860-850 Ma rock suites were generated in a convergent plate margin and are part of the Jiangnan belt, and not the Cathaysia Block, thus constraining the location of the suture between the two lithotectonic units in NE Zhejiang area during Neoproterozoic.

Keywords: Jiangshan-Shaoxing fault zone; quartz diorite; Geochronology; Neoproterozoic arc suites; tectonic affinity; South China

1. Introduction

The Neoproterozoic Jiangshan-Shaoxing fault zone delineates the SE margin of the Jiangnan orogenic belt, which is an assemblage of Neoproterozoic convergent plate margin accretionary successions that record the assembly of the Cathaysia and Yangtze blocks in South China Craton (Fig. 1; Cawood et al., 2013). The age and nature of the arc-trench successions as well as their number and direction of subduction, along with the overall crustal evolution of the orogenic belt and timing of final assembly between Yangtze and Cathaysia blocks, are disputed (Shu, 2012;

Wang et al., 2014; Yao et al., 2014a, b, 2015; Zhao, 2015). This uncertainty in the evolution of the orogen has resulted in controversy as to whether South China occupies an internal or marginal position in the Rodinia supercontinent (Cawood et al., 2013; Wang et al., 2013b).

The northeast-southwest trending Jiangshan-Shaoxing fault zone can be traced for up to 800 km and is up to 30 km wide (Shu, 2012). The fault is considered to constitute the southeastern boundary of the Jiangnan orogen with the Cathaysia Block. In the vicinity of Shijiao (Zhejiang Province), within the fault zone, constituent rock suites are similar to those of the Jiangnan belt, but metamorphic grade is higher and similar to that in the adjoining Chencai metamorphic complex to the southeast, which forms part of the Cathaysia Block (Fig. 2, BGMRZJ, 1989; Zhao and Sun, 1994), or alternatively has been interpreted to form the NE extent of the Jiangshan-Shaoxing fault zone as a Neoproterozoic suture (Shu et al., 2006). These relations have led to suggestions that the rocks within the fault zone may constitute part of supra-subduction zone units on the margin of the Cathaysia Block (e.g., Zhao, 2015). This in turn has implications for the Neoproterozoic crustal evolution of South China and, in particular, whether southeast-directed subduction took place beneath the margin of the Cathaysia Block (e.g., Wang et al., 2014; Zhao, 2015). Our study outlines field, geochemical and isotopic data on migmatized quartz diorite and mafic-ultramafic rocks in the fault zone, along with volcanic rocks and associated sedimentary rocks of the adjoining Shuangxiwu Group from the Jiangnan belt to the northwest (Fig. 2). Our results indicate that fault zone lithologies are an accretionary

assemblage within the Jiangnan belt rather than the Cathaysia Block, thus delinating the boundary between the two lithotectonic assemblages at Shijiao. Furthermore, they demonstrate the presence of ca. 880 to 850 Ma convergent plate margin units in the eastern Jiangnan belt, providing an additional constraint on the age of final assembly between Yantze and Cathaysia blocks.

2. Geological setting and litho-stratigraphic structures

2.1. Geological setting

The South China Craton consists of the Yangtze Block to the northwest and Cathaysia Block to the southeast, sutured along the Jiangnan orogenic belt. The former is composed of an Archean–Paleoproterozoic crystalline basement surrounded by Neoproterozoic orogenic belts (Panxi-Hannan belt and Jiangnan belt) that underwent mid-Neoproterozoic greenschist facies metamorphism (Fig. 1; Shu, 2012; Zhao and Cawood, 2012). These units are overlain by middle-late Neoproterozoic to Phanerozoic strata (Charvet et al., 2010; Wang et al., 2013a, 2014; Dong et al., 2015). The Cathaysia Block contains numerous Neoproterozoic-Paleozoic meta-sedimentary and meta-igneous rocks, as well as minor Paleoproterozoic meta-igneous rocks (Zhao and Cawood, 2012; Shu, 2012; Shu et al., 2014, 2015). Paleozoic regional metamorphism of amphibolite facies along with coeval deformation, crustal partial melting and granite emplacement, are distinctive features of the Cathaysia Block compared to the Jiangnan belt (Shu, 2006; Li et al., 2010).

2.1. Lithology and related structures

The greenschist facies early Neoproterozoic Shuangxiwu Group (Pt3sh) is the oldest unit exposed in the eastern Jiangnan belt in northern Zhejiang Province, and is unconformably overlain by a northwest dipping middle Neoproterozoic succession, the Heshangzheng Group (Pt3h), and the latest Neoproterozoic Sinian System (Pt3z) that are essentially unmetamorphosed (Fig. 2, 3a, 3b; BGMRZJ, 1989). The Shuangxiwu Group is divided into the Pingshui, Beiwu, Yanshan and Zhangcun formations. The Pingshui and Yanshan formations consist predominantly of intermediate-acidic volcanic rocks, whereas the Beiwu Formation is composed mainly of intermediate-basic volcanic rocks. The Zhangcun Formation contains a series of continental derived sedimentary rocks (tuff and tuffaceous sandstones and siltstones) (BGMRZJ, 1989). The volcanic rocks from the Pingshui Formation are dated at 978 ± 44 Ma (Sm–Nd whole rock isochron, Zhang et al., 1990) and 904 ± 8 Ma and 906 ± 10 Ma (LA-ICPMS U–Pb zircon, Chen et al., 2009). Andesitic rocks from the Beiwu and Zhangcun formations yield discordant U-Pb $^{206}Pb/^{238}U$ zircon ages of 926 ± 15 Ma and 891 ± 12 Ma (Li et al., 2009). The unconformably overlying middle Neoproterozoic Heshangzheng Group has a maximum depositional age of ca. 820 Ma as constrained by detrital zircons (Yao et al., 2013). It consists of an interstratified succession of conglomerate, sandstone, siltstone and mudstone, with interbedded tuff and muddy limestone Fig. 3).

In the Shijiao area, within the Jiangshan-Shaoxing fault zone, exposed rock units are mainly migmatized hornblende schist intruded by migmatized quartz diorite, along with minor meta-rhyolite (Fig. 2). Amphibole pyroxenite along with minor

gabbro and dunite occur as blocks within the quartz diorite (Fig. 4). Minor nodular ultramafic rocks occur in the transition zone between ultramafic rocks and migmatized quartz diorite (Zhou et al., 1993). Rock units within the fault zone are metamorphosed to amphibolite facies. Zircon ages of 879 ± 10 Ma (LA-ICPMS U–Pb; Yao et al., 2014a) and 838 ± 5 Ma (SHRIMP U-Pb; Li et al. (2010) have been obtained from the hornblende schist and meta-rhyolite, respectively. Local mylonitization also occurs in the diorite and has been dated at 370 ± 10 Ma (K–Ar on biotite), 353 Ma and 361 Ma (Ar–Ar on biotite, with unknown errors and data quality cannot be evaluated) (Zhu and Zhou, 1994).

The Chencai metamorphic complex, which lies to the southeast of the Jiangshan-Shaoxing fault zone (Fig. 1, Fig. 2; BGMRZJ, 1989), consists of plagioclase gneiss, amphibolite, and leucocratic gneiss interbanded with schist, leptynite, marble and minor quartzite (BGMRZJ, 1989). Protoliths of the complex are considered to be Neoproterozoic in age that experienced Paleozoic amphibolite facies metamorphism and coeval deformation (Yao et al., 2014a; Shu et al., 2015). The unit also shows widespread migmatization. Zircon SHRIMP U–Pb ages of 857 ± 7 and 841 ± 12 are reported from meta-gabbro within the complex (Li et al., 2010; Shu et al. 2011). An intercept age of 1781 ± 21 Ma inferred from SHRIMP zircon U–Pb ages has also been obtained from amphibolite and interpreted as the formation age of gabbroic protolith (Li et al., 2010). Metamorphism is dated at 426 ± 2 Ma based on $^{40}Ar/^{39}Ar$ age on hornblende and 426 ± 7 Ma by $^{40}Ar/^{39}Ar$ age on biotite (Li et al., 2010). Zircon U–Pb ages of 453 ± 4 Ma and 438 ± 4 Ma are reported from the

142 migmatite and gabbro inclusions within the Chencai Complex (Yao et al. 2014a).

143 ***2.2. Sample descriptions***

144 Sample locations are shown on figures 2 and 3 and include 2 quartz diorites (1194
145 and 1194-1; GPS: N25°45.919', E109°50.071') and 12 mafic-ultramafic rocks (1472,
146 1472-4, 1472-6, 1472-7, 1472-8, 1472-11, 1472-12, 1472-13, 1472-14, 1472-15,
147 1472-17 and 1472-18; GPS: N29°33.220', E120°10.296') from within the
148 Jiangshan-Shaoxing fault zone (Fig. 2). Two andesitic porphyrite samples (1468-1,
149 1468-4; GPS: N29°54.064', E119°58.437'), one pyroclastic sample (1470; GPS:
150 N29°52.533', E120°01.268') and one basalt sample (1467-2; GPS: N29°52.533',
151 E120°01.268') were also collected from the Shuangxiwu Group (Fig. 2, Fig. 4).

152 The quartz diorite samples 1194, 1194-1 contain about 65% plagioclase, 20%
153 hornblende and 15% quartz. Gabbro sample 1472 contains some 60% plagioclase,
154 25% clinopyroxene, 10% hornblende, 5% opaque mineral oxide and other accessory
155 mineral such as titanite, whereas gabbro sample 1172-4 has 35% plagioclase, 45%
156 clinopyroxene and 5% olivine, along with 10% hornblende and 5% accessory
157 minerals (opaque oxide). Other gabbro samples 1472-07, 1472-12, 1472-13, 1472-15,
158 and 1472-18 are mainly composed of 15~25% plagioclase, 50~65% clinopyroxene
159 and 10% hornblende. Amphibole pyroxenite samples 1472-6, 1472-8, 1472-11,
160 1472-14 and 1472-17 contain about 60% clinopyroxene, 30% hornblende and 10%
161 magnetite and other accessory minerals. Two andesitic porphyrite samples (1468-1,
162 1468-4) mainly contain phenocrysts of plagioclase, which occur in a fine grained to
163 glassy matrix. The pyroclastic rock sample (1470) is foliated and composed of

muscovite, quartz, plagioclase and rock fragments (Fig. 5).

The diorite samples (1194 and 1494-1) and gabbro sample 1472 were selected for zircon U–Pb dating and Hf isotope analysis. These along with the remaining samples were analyzed for whole rock geochemistry.

3. Analytical procedures

Zircons were separated from the crushed rocks using heavy liquid and magnetic techniques and then handpicked under a binocular microscope. The zircon grains were mounted in epoxy resin, polished and coated. Cathodoluminescence (CL) images of the zircons were obtained using a Quanta 400 FEG electron microscope equipped with Mono CL3+ (Gatan, U.S.A.) at the State Key Laboratory of Continental Dynamics in Northwest University.

The zircon U–Pb isotopic dating was carried out at the State Key Laboratory for Mineral Deposits Research in Nanjing University, using an Agilent 7500a ICP–MS connected to a New Wave 213 nm laser ablation system. U–Pb fractionation was corrected using zircon standard GEMOC GJ–1 with an age of 601 ± 12 Ma and accuracy was controlled by using the zircon standard Mud Tank with an age of 735 ± 12 Ma. The U–Pb ages were calculated from the original signal data using the Glitter software and U–Th–Pb age data are plotted on concordia diagrams using the Isoplot program (Ludwig, 2003). Zircons older than 1000 Ma have high contents of radiogenic Pb, hence $^{207}Pb/^{206}Pb$ age is more reliable and used to determine the crystallization age. On the other hand, due to low content of radiogenic Pb, the $^{206}Pb/^{238}U$ age is more reliable for zircons with ages younger than 1000 Ma.

The zircon Hf isotopes were analyzed using a Neptune MC–ICP–MS at the State Key Laboratory for Mineral Deposits Research in Nanjing University. Zircon standard 91500 was used for external correction and has a $^{176}Hf/^{177}Hf$ value of 0.282300 ± 8 (2σ). Initial $^{176}Hf/^{177}Hf$ values were calculated based on Lu decay constant of 1.865E–11 (Scherer et al., 2001). The Hf model ages were calculated under the assumption that the $^{176}Lu/^{177}Hf$ of average crust is 0.015, and the $^{176}Hf/^{177}Hf$ and $^{176}Lu/^{177}Hf$ ratios of chondrite and depleted mantle at the present time are 0.282772 and 0.0332, 0.28325 and 0.0384 (Blichert-Toft and Albarede, 1997).

Whole rock major element analyses were performed using an ARL9800XP+ X–ray fluorescence spectrometer (XRF) at the State Key Laboratory for Mineral Deposits Research in Nanjing University. The analytical precision is generally better than 2% for all elements. Trace element abundances were measured using a Finnigan Element II ICP–MS at the State Key Laboratory of Mineral Deposit Research, Nanjing University, which gives precision better than 10% for most of the analyzed elements.

4. Analytical results

4.1. Zircon U–Pb dating and Hf isotopes

Zircons obtained from gabbro (1472) and diorite (1194, 1194-1) samples are mostly euhedral prismatic grains. Most of the grains show banded or sector zoning in CL images (Fig. 6). A total of 32 grains from gabbro sample 1472 were analyzed, yielding a main age range of 953–847 Ma and giving a weighted average $^{206}Pb/^{238}U$

age of 860 ± 5 Ma (MSWD = 0.08, n = 24) (Fig. 6). Among twenty-two analyses from quartz diorite sample 1194, 18 U–Pb dating analyses yield a weighted average $^{206}Pb/^{238}U$ age of 854 ± 6 Ma (MSWD = 0.2, n = 18) (Fig. 6). Twenty analyses were conducted on zircons from gabbro sample 1472, yielding an age range of 871–857 Ma and a weighted average $^{206}Pb/^{238}U$ age of 857 ± 5 Ma (MSWD = 0.24, n = 20). These weighted mean ages are interpreted as the crystallization age of the gabbro and diorite samples. The Th/U ratios of the zircons from gabbro and diorite sample range from 0.66 to 3.39 and 0.75 to 1.57, respectively (Table 1).

Zircons from quartz diorite samples 1194 and 1194-1 display present day $^{176}Hf/^{177}Hf$ ratios of 0.282378–0.282558 and yield positive εHf(t) values of 7.81~11.8 and 4.57~10.42, respectively (Table 2). This equates to Hf model ages of 1.0~1.2 Ga (Figure. 7), suggesting the presence of latest Mesoproterozoic juvenile mantle material in this region.

4.2. Major and trace element compositions

Major and trace element analytical results are presented in Table 3. Our discussion focuses mainly on the immobile elements and element ratios due to low-grade alteration of the rock units and the possibility of mobilization of elements with a large ionic radius to charge during low-grade metamorphism (Pearce and Cann, 1973; Wood, 1980; Wyman, 1999). On the Zr/TiO_2–Nb/Y diagram, the studied samples fall in the basalt and andesite field (Fig. 8).

The quartz diorite samples (1194 and 1194-1) have low TiO_2 (0.62 %), SiO_2 (55.56–55.83 %) and Na_2O (4.61–4.63 %), with high Mg# of 49 (Table 3). The coarse

grained gabbros (1472) also display low values of TiO_2 (1.02 %), SiO_2 (44.9 %) and Na_2O (0.72 %), with Mg# of 49. Other mafic and ultramafic rock samples from the Shijiao area within the Jiangshan-Shaoxing fault zone display a wide range of compositions of SiO_2 (33.33 to 53.46 %), MgO (9.93–23.4 %) and FeO^t (12.09–26.52%), and low Al_2O_3 (3.79–7.96%) (Table 3). All mafic-ultramafic intrusive rocks and diorites in the fault zone show minor LREE enriched patterns and minor Eu anomalies with Eu/Eu* ratios of 0.61–1.25 (Fig. 8). On primitive mantle–normalized plots, the investigated samples display enrichment in Th, Pb and variable depletion in high field strength elements (HFSE) such as Nb, Ta, Zr, Hf, Ti and Rb (Fig. 8). The andesitic porphyrite and basalt samples from the Shuangxiwu Group show features that are similar to those within the fault zone (Fig. 9, 10). The andesitic porphyrite samples (1468 and 1468-1) have SiO_2 content of 60.4~67.6 %, CaO of 0.05~1.31 %, Na_2O of 1.65~5.42 % and K_2O of 1.09~7.73 %, with K_2O/Na_2O of 0.2 to 4.68 (Table 3). The basalt sample (1467) from the Shuangxiwu Group in the Jiangnan belt displays a SiO_2 content of 50.02 %, CaO of 9.95 %, Na_2O of 3.34 % and K_2O of 1.15 %. The basaltic rocks and andesitic porphyrite samples yield LREE enriched patterns with minor depletion of Eu (Eu/Eu* ratios of 0.77~0.94). Depletion of Ti, Sr, Nb, Ta and enrichment of Rb, Th, Pb are also observed, similar to those from the fault zone at Shijiao (Fig. 8), trace element patterns from pyroclastic rock samples are also similar to those from the fault zone at Shijiao.

5. Discussion

253 ***5.1. Field geology, petrology and geochemistry***

254 Within the Jiangshan-Shaoxing fault zone at Shijiao, migmatized diorite intrudes
255 the hornblende schist, and coarse-grained ultramafic rocks and gabbro occur as
256 inclusions in the migmatized quartz diorite. Age data are consistent with field
257 observations. The hornblende schist and mafic-ultramafic inclusions were generated
258 at ca. 880 Ma (888 ± 10 Ma, K–Ar hornblende, Zhou and Zhu, 1992; 879 ± 10 Ma,
259 LA-ICPMS U–Pb gabbro, Yao et al., 2014a), and is older than the formation of quartz
260 diorite (ca. 850 Ma).

261 Rock units exposed to the northwest of the fault zone are the typical volcanic
262 rocks of the Shuangxiwu Group (ca. 990~880 Ma), the lower part of which are
263 intruded by 913~905 Ma I-type granitoids (Fig. 2; Ye et al., 2007; Li et al., 2009). On
264 the other hand, the Chencai Complex of the Cathaysia Block is composed mainly of
265 pelitic sedimentary rocks with minor mafic rocks and experienced Paleozoic
266 metamorphism of amphibolite facies. Southeast-directed thrusts occur within the
267 complex and are assumed to be Paleozoic, synchronous with metamorphism but have
268 not been directly dated (Li et al., 2010).

269 Geochemical data suggests formation of rock units within the
270 Jiangshan-Shaoxing fault zone at Shijiao area in a convergent plate margin setting.
271 The migmatized quartz diorite samples show a depletion in high field strength
272 elements (HFSE) such as Nb, Ta, Zr, Hf and Ti compared with their neighboring
273 elements (Fig. 9), similar to those formed in an island arc setting (Wyman, 1999).
274 Mafic-ultramafic intrusive rocks that occur as inclusions within the migmatized

diorite also display similar geochemical features. Pyroclastic and basaltic rocks from the Shuangxiwu Group in the eastern Jiangnan belt likewise display geochemical signatures typical of a convergent plate margin setting (Fig. 9). On tectonic discrimination diagrams, such as Ti–Zr plot of Peace and Cann (1973), Y–La–Nb plot of Wood (1980) and Cr–Y plot of Pearce et al. (1982) (Fig. 10), most of the investigated samples plot in the field of arc basalts. The quartz diorite samples from the fault zone display obvious Nb–Ta depletion, which is indicative of volcanic arc geochemical signature, as well as the andesitic porphyrite from the Shuangxiwu Group. These features are comparable to those of the typical Shuangxiwu arc (Li et al., 2009). Thus, based on rock assemblages, field geology and geochemical data, we infer that the migmatized quartz diorite and mafic-ultramafic rocks caught within the Jiangshan-Shaoxing fault zone at Shijiao were generated in a convergent margin setting, similar to the protolith of the amphibolite schist in the studied area (Yao et al., 2014a) and also similar to rock units of the Shuangxiwu Group in the Jiangnan belt (Li et al., 2009).

5.2. Tectonic implications

Geological, geochronological and geochemical features of rock units within the Jiangshan-Shaoxing fault zone in the Shijiao area include a suite of quartz diorite and meta-mafic-ultramafic rocks and hornblende schist with ages around 880-850 Ma, and a convergent plate margin magmatic arc geochemical signature. Furthermore, these features are comparable to those of the adjoining but lower greenschist facies metamorphic rocks of the Shuangxiwu Group, which is also interpreted as part of a ca.

1000-880 Ma magmatic arc (Shu and Charvet, 1996; Charvet et al., 1996; Chen et al., 2009; Li et al., 2009).

The subduction direction of oceanic crust between the Yangtze and Cathaysia blocks has generally been considered to be northwestward beneath the Jiangnan arc (also referred to as 'Shuangxiwu arc' or 'Huaiyu arc') in SE margin of the Yangtze Block (Shu and Charvet, 1996). The supra-subduction zone Northeast Jiangxi Ophiolite, which is exposed between an arc assemblage and the continental Yangtze Block, is suggested as a relic of the back-arc basin (Shu and Charvet, 1996; Li et al., 1997). The subduction direction of the back-arc basin in its latest stage has also been suggested to be northwestward as constrained by analysis of inferred ca. 930-900 Ma ductile deformation fabrics from areas in and adjacent the Northeast Jiangxi suture zone (Shu and Charvet, 1996). Recent work has also suggested the presence of Neoproterozoic southwestward subduction beneath the NE margin of the Cathaysia Block (Wang et al., 2014; Zhao, 2015). The arc type rock suites in the fault zone at Shijiao area, if they belong to the Cathaysia Block (cf. Shui et al., 1986; Li et al., 2010), could serve as the evidence of a magmatic arc on the northeastern margin of the Cathaysia Block related to southwestward-directed subduction beneath the margin. Thus, the affinity of the rock suites within the Jiangshan-Shaoxing fault zone can help constrain the number and direction of subduction zones associated with assembly of the Yangtze and Cathaysia blocks.

The ca. 880–850 Ma arc type rock units within Jiangshan-Shaoxing fault zone at Shijiao area indicate this area differs from the Chencai Complex. The complex has a

protolith dominated by continental derived materials metamorphosed at ca. 426 Ma (Li et al., 2010), along with minor meta-mafic rocks which have yielded ages of ca. 858 Ma and ca. 438 Ma with the former displaying within plate geochemical affinities (Shu et al., 2011; Yao et al., 2014a). The amphibolite-grade metamorphism in the fault zone most likely reflects the proximity to the Cathaysia Block, which underwent widespread early Paleozoic metamorphism (Shu et al., 2014, 2015), as inferred from mylonitization dated at ca. 421–398 Ma (Ar-Ar, Shu et al., 1999). On the other hand, the ca. 1000-880 Ma arc type meta-magmatic rocks of the Shuangxiwu Group are similar to those within Jiangshan-Shaoxing fault zone at Shijiao. Moreover, given that the middle to late Neoproterozoic Sinian System and Heshangzheng Group unconformably overlie the Shuangxiwu Group and show little to no metamorphism and deformation (BGMRZJ, 1989), then the metamorphism and deformation of the Shuangxiwu Group must be Neoproterozoic. Therefore, the Paleozoic amphibolite facies metamorphism in the fault zone does not conflict with Neoproterozoic greenschist facies metamorphism of the eastern Jiangnan belt and with the mostly accepted NW-ward accretionary subduction beneath Jiangnan belt (Charvet et al., 1996; Shu and Charvet, 1996; Cawood et al., 2013).

In this study, we suggest the andesitic and mafic-ultramafic rocks within the Jiangshan-Shaoxing fault zone at Shijiao belong to the Jiangnan orogenic belt and were produced in a convergent plate margin at ca. 880–850 Ma (Fig. 11). These results indicate that the previously proposed ca. 980–880 Ma convergent plate margin setting in the eastern Jiangnan belt (Ye et al., 2007; Li et al., 2009) lasted at least to ca.

850 Ma and is consistent with the overall duration of the convergent plate margin geochemical signature preserved within the Jiangnan belt (Shu et al., 1994, 2006; Zhao and Cawood, 2012; Cawoodet al, 2013; Zhang et al., 2013; Yao et al., 2015). Data on the age and origin of S-type granites within the Jiangnan orogenic belt along with the overall Neoproterozoic stratigraphic sequence that includes deformed and metamorphosed older units and younger unconformably overlying little deformed and unmetamorphosed middle to late Neoproterozoic units, constrains final assembly of the Yangtze and Cathaysia blocks to sometime between ca. 850-810 Ma (e.g. Wang et al., 2007, 2012; Zhao and Cawood, 2012; Yao et al., 2014b).

We believe the lithologies within the Jiangshan-Shaoxing fault zone at Shijiao formed in a subduction zone setting and do not belong to the Cathaysia Block, and therefore cannot be used as indicators for southeastward subduction of oceanic crust beneath the NE margin of Cathaysia Block. The fault along the NE margin of Chencai Complex constitutes the boundary of Cathaysia Block and Jiangnan belt at Shijiao. Field, age and geochemical relationships of this study argue against models suggesting ca. 880 Ma collision and ca. 860 Ma rifting of the South China Craton (e.g. Li et al., 2008). Our data require a younger assembly age, at least after ca. 850 Ma and a marginal position for South China within the Rodinia supercontinent (Cawood et al., 2013; Wang et al., 2014).

6. Conclusions

The ca. 880~850 Ma quartz diorite, mafic-ultramafic rocks and hornblende schist

identified from within the Jiangshan-Shaoxing fault zone at Shijiao area are indicative of a convergent plate margin setting. Lithology, structure, age data, geochemistry and metamorphic grade indicate the rocks units in Shijiao area display close affinity with the Jiangnan belt rather than the Cathaysia Block. The investigated rock units formed around 880~850 Ma in a convergent plate margin setting in the eastern Jiangnan belt and do not provide evidence for Neoproterozoic subduction of oceanic crust beneath the NE margin of the Cathaysia Block. The Jiangshan-Shaoxing fault zone at Shijiao marks the NE margin of the Chencai Complex of the Cathaysia Block and delineates the boundary between the block and the Jiangnan belt.

Acknowledgements

Reviews by Dr. Sanzhong Li and Dr. Wenjiao Xiao are gratefully acknowledged. We also thank Dr. Y.H. Yang and J.Q. Wang for their help with zircon dating and Hf isotopic data collection. We acknowledge the financial support provided by the National Basic Research Program of China (973 Program, No. 2012CB416701), the National Natural Science Foundation of China (Nos. 41330208, 41572200, 41272226) and the Bureau of China Geological Survey (No. 1212011121064-01).

References

BGMRZJ (Bureau of Geology and mineral Resources Jiangxi Province), 1989. Regional Geology of Jiangxi Province. Geology Publishing House, Beijing, 5–575 (In Chinese with English Abstract).

Blichert-Toft, J., Albarede, F., 1997. The Lu–Hf isotope geochemistry of chondrites and the evolution of the mantle–crust system. Earth and Planetary Science Letters 148, 243–258.

Cawood, P.A., Wang, Y.J., Xu, Y.J., Zhao, G.C., 2013. Locating South China in Rodinia and Gondwana: a fragment of Greater Indian Lithosphere? Geology 41(8), 903–906.

Charvet, J., Shu, L.S., Shi, Y.S., Guo, L.Z., Faure, M., 1996. The building of south China: collision of Yangtze and Cathaysia blocks, problems and tentative answers. Journal of Southeast Asian Earth Sciences 13 (3–5), 223–235.

Charvet, J., Shu, L.S., Faure, M., Choulet, F., Wang, B., Lu, H.F., Le Breton, N., 2010.Structural development of the Lower Paleozoic belt of South China: Genesis of an intracontinental orogen. Journal of Asian Earth Sciences 39, 309–330.

Chen, Z.H., Xing, G.F., Guo, K.Y., Dong, Y.G., Chen, R., Zeng, Y., Li, L.M., He, Z.Y., Zhao, L., 2009. Petrogenesis of the Pingshui keratophyre from Zhejiang: Zircon U–Pb age and Hf isotope constraints. Chinese Science Bulletin 54, 610–617 (in Chinese with English abstract).

Dong, S.W., Zhang, Y.Q., Gao, R., Su, J.B., Liu, M., Li, J.H., 2015. A possible buried Paleoproterozoic collisional orogen beneath central South China: Evidence from seismic-reflection profiling. Precambrian Research 264, 1–10.

Li, X.H., Zhao, J.X., McCulloch, M.T., Zhou, G.Q., Xing, F.M., 1997. Geochemical and Sm-Nd isotopic study of Neoproterozoic ophiolites from southeastern China: petrogenesis and

403 tectonic implications. Precambrian Research 81, 129-144.

404 Li, X.H, Li, W.X., Li, Z.X., Lo, C.H., Wang, J., Ye, M.F., Yang, Y.H., 2009. Amalgamation
405 between the Yangtze and Cathaysia Blocks in South China: Constraints from SHRIMP U–Pb
406 zircon ages, geochemistry and Nd–Hf isotopes of the Shuangxiwu volcanic rocks.
407 Precambrian Research 174, 117–128.

408 Li, Z.X., Bogdanova, S.V., Collins, A.S., Davidson, A., De Waele, B., Ernst, R.E., Fitzsimons,
409 I.C.W., Fuck, R.A., Gladkochub, D.P., Jacobs, J., Karlstrom, K.E., Lu, S., Natapov, L.M.,
410 Pease, V., Pisarevsky, S.A., Thrane, K., Vernikovsky, V., 2008. Assembly, configuration,
411 and break-up history of Rodinia: a synthesis. Precambrian Research 160, 179–210.

412 Li, Z.X., Li, X.H., Wartho, J.A., Clark, C., Li, W.X., Zhang, C.L., Bao, C.M., 2010. Magmatic
413 and metamorphic events during the early Paleozoic Wuyi□Yunkai orogeny, southeastern
414 South China: New age constraints and pressure-temperature conditions. Geological Society
415 of America Bulletin 122 (516), 772–793.

416 Ludwig, K.R., 2003. Isoplot 3.00, a geochronological Toolkit for Microsoft Excel. Berkeley
417 Geochronology Center, Special Publication 4, 1-70.

418 McDonough, W.F., Sun, S.S., 1995. Composition of the Earth. Chemical Geology 120, 223-253.

419 Mullen, E.D., 1983. MnO/TiO2/P2O5—a minor element discriminant for basaltic rocks of oceanic
420 environments and implication for petrogenesis. Earth Planet Science Letters 62, 53–62.

421 Pearce, J.A., Cann, J.R., 1973. Tectonic setting of basic volcanic rocks determined using trace
422 element analyses. Earth and Planetary Science Letters 19, 290-300.

423 Pearce, J.A., 1982. Trace element characteristics of lavas from destructive plate boundaries. In:
424 Thorpe, R.S. (Ed.), Andesites. Wiley, New York, pp. 525–548.

425 Pearce, J.A., Harris, N.B.W., Tindle, A.G., 1984. Trace element discrimination dia-grams for the

tectonic interpretation of granitic rocks. Journal of Petrology 25,956–983.

Scherer, E., Munker, C., Mezger, K, 2001. Calibration of the Lutetium–Hafnium clock. Science 293, 683–687.

Shu, L.S., 2006. Predevonian Tectonic Evolution of South China: from Cathaysian Block to Caledonian Period Folded Orogenic Belt. Geological Journal of China Universities 12(4), 418-431. (In Chinese with English abstract)

Shu, L.S., 2012. An analysis of principal features of tectonic evolution in South China Block. Geological Bulletin of China 31(7), 1035-1053.

Shu, L.S., Zhou, G.Q., Shi, Y.S., Yin, J., 1994. Study on the high pressure metamorphic blueschist and its Late Proterozoic age in the Eastern Jiangnan belt. Chinese Science Bulletin 39, 1200–1204.

Shu, L.S., Charvet, J., 1996. Kinematics and geochronology of the Proterozoic Dongxiang - Shexian ductile shear zone: with HP metamorphism and ophiolitic melange (Jiangnan region, South China). Tectonophysics 267, 291–302.

Shu, L.S., Lu, H.F., Jia, D., Charvet, J., Faure, M., 1999, Study of the 40Ar/39Ar isotopic age for the early Paleozoic tectonothermal event in the Wuyishan region, South China. Journal of Nanjing University (Natural Science) 35(6), 668-674 (In Chinese with English abstract).

Shu, L.S., Faure, M., Jioang, S.Y., Yang, Q., Wang Y.J., 2006. SHRIMP zircon U-Pb age, litho- and biostratigraphic analyses of the Huaiyu Domain in South China - Evidence for a Neoproterozoic orogen, not Late Paleozoic-Early Mesozoic collision. Episodes 29(4), 244-252.

Shu, L.S., Faure, M., Yu, J.H., Jahn, B.M., 2011. Geochronological and geochemical features of the Cathaysia Block (South China): New evidence for the Neoproterozoic breakup of Rodinia.

449 Precambrian Research 187 (3–4), 263–276.

450 Shu, L.S., Jahn, B.M., Charvet, J., Santosh, M., Wang, B., Xu, X.S., and Jiang, S.Y., 2014. Early
451 Paleozoic depositional environment and intracontinental orogeny in the Cathaysia Block
452 (South China): implications from stratigraphic, structural, geochemical and geochronologic
453 evidence. American Journal of Science 314, 154-186.

454 Shu, L., Wang, B., Cawood, P. A., Santosh, M., Xu, Z.Q., 2015. Early Paleozoic and early
455 Mesozoic intraplate tectonic and magmatic events in the Cathaysia Block, South China.
456 Tectonics 34, 1600-1621.

457 Shui, T., Xu, B.T., Liang, R.H., Qiu, Y.S., 1986. Shaoxing-Jiangshan deep-seated fault zone,
458 Zhejiang Province. Chinese Science Bulletin 31(18), 1250–1255.

459 Sun, S.S., McDonough, W.F., 1989. Chemical and isotopic systematics of oceanic basalts:
460 implication for mantle composition and processes. In: Saunder, A.D., Norry, M.J. (Eds.),
461 Magmatism in the Ocean Basins: Geological Society, London, Special Publications 42,
462 313–345.

463 Wang, J., Deng, Q., Wang, Z. J., 2013a. New evidence for sedimentary attributes and timing of
464 the “Macaoyuan Group conglomerates” on the northern margin of the Yangtze block in
465 southern China. Precambrian Research 235, 58-70.

466 Wang, W., Zhou, M.F., Yan, D.P., Li, J.W., 2012. Depositional age, provenance, and tectonic
467 setting of the Neoproterozoic Sibao Group, southeastern Yangtze Block, South China.
468 Precambrian Research 192–195, 107–124.

469 Wang, X.L., Zhou, J.C., Griffin, W.L., Wang, R.C., Qiu, J.S., O’Reilly, S.Y., Xu, X.S., Liu, X.M.,
470 Zhang, G.L., 2007. Detrital zircon geochronology of Precambrian basement sequences in the

471 Jiangnan orogen: Dating the assembly of the Yangtze and Cathaysia Blocks. Precambrian
472 Research 159, 117–131.
473 Wang, Y.J., Zhang, A.M., Cawood, P.A., Fan, W.M., Xu, J.F., Zhang, G.W., Zhang, Y.Z., 2013b.
474 Geochronological, geochemical and Nd-Hf-Os isotopic fingerprinting of an early
475 Neoproterozoic arc-back-arc system in South China and its accretionary assembly along the
476 margin of Rodinia. Precambrian Research 231, 343–371.
477 Wang, Y.J., Zhang, Y.Z., Fan, W.M., Geng, H.Y., Zou, H.P., Bi, X.W., 2014. Early
478 Neoproterozoic accretionary assemblage in the Cathaysia block: geochronological, Lu–Hf
479 isotopic and geochemical evidence from granitoid gneisses. Precambrian Research 249,
480 144–161.
481 Wyman, D. A., 1999. A 2.7 Ga depleted tholeiite suite: evidence of plume-arc interaction in the
482 Abitibi Greenstone belt, Canada. Precambrian Research 97, 27–42.
483 Wood, D.A., 1980. The application of a Th–Hf–Ta diagram to problems of tecto-magmatic
484 classification and to establishing the nature of crustal contamination of basaltic lavas of the
485 British Tertiary volcanic province. Earth Planet Science Letters 50, 11–30.
486 Yao, J.L., Shu, L.S., Santosh, M., Li, J.Y., 2013. Geochronology and Hf isotope of detrital zircons
487 from Precambrian sequences in the eastern Jiangnan Orogen: Constraining the assembly of
488 Yangtze and Cathaysia Blocks in South China. Journal of Asian Earth Sciences 74, 225–243.
489 Yao, J.L., Shu, L.S., Santosh, M., Xu, Z.Q., 2014a. Palaeozoic metamorphism of the
490 Neoproterozoic basement in NE Cathaysia: zircon U–Pb ages, Hf isotope and whole-rock
491 geochemistry from the Chencai Group. Journal of the Geological Society, London 171,
492 281–297.

493 Yao, J.L, Shu, L.S., Santosh, M., Zhao, G.C., 2014b. Neoproterozoic arc-related mafic-ultramafic
494 rocks and syn-collision granite from the western segment of the Jiangnan Orogen, South
495 China: constraints on the Neoproterozoic assembly of the Yangtze and Cathaysia Blocks.
496 Precambrian Research 243, 39– 62.
497 Yao, J.L., Shu, L.S., Santosh, M., Li, J.Y., 2015. Neoproterozoic arc-related andesite and
498 orogeny-related unconformity in the eastern Jiangnan orogenic belt: Constraints on the
499 assembly of the Yangtze and Cathaysia blocks in South China. Precambrian Research 262,
500 84–100.
501 Ye, M.F., Li, X.H., Li, W.X., Liu, Y., Li, Z.X., 2007. SHRIMP zircon U–Pb geochronological and
502 whole-rock geochemical evidence for an early Neoproterozoic Sibaoan magmatic arc along
503 the southeastern margin of the Yangtze Block. Gondwana Research 12, 144–156.
504 Zhang, B.T., Ling, H.F., Shen,W.Z., Liu, J.S., Yang, J.D., Tao, X.C., 1990. Sm–Nd isochronic age
505 of spilite-keratophyre of Shuangxiwu Group in Xiqiu, Shaoxing, Zhejiang Province. Journal
506 of Nanjing University (Earth Science) 2, 9–14 (in Chinese with English Abstract).
507 Zhang, Y.Z., Wang, Y.J., Geng, H.Y., Zhang, Y.H., Fan, W.M., Zhong, H., 2013. Early
508 Neoproterozoic (850 Ma) back-arc basin in the Central Jiangnan Orogen (Eastern South
509 China): Geochronological and petrogenetic constraints from meta-basalts. Precambrian
510 Research 231, 325-342.
511 Zhao, G.C., 2015. Jiangnan Orogen in South China: Developing from divergent double subduction.
512 Gondwana Research 27(3), 1173–1180.
513 Zhao, G.C., Cawood, P.A., 2012. Precambrian geology of China. Precambrian Research 222–223,
514 13–54.

515 Zhao, G.C. Sun, D.Y., 1994. The studies on metamorphic stages and metamorphic PTD path of
516 Chencai Group, southwestern Zhejiang province. Journal of Changchun University of Earth
517 Sciences 24(3), 246-253 (In Chinese with English abstract).
518 Zhou, X.M., Zhu, Y.H., Chen, J.G., 1993. Discovering of nodule ultramafic rocks and it's genesis.
519 Chinese Science Bulletin, 604-604.
520 Zhou X M, Zhu Y H., 1992. Magma mixing in the Jiang-Shao fault zone and the Precambrian
521 geology of both side of the Jiang-Shao zone (in Chinese with English abstract). Science in
522 China Series B 22, 298–303.
523 Zhu, Y.H., Zhou, X.M., 1994. Mylonitization of diorite in Jiangshao fracture belt Zhejiang
524 province. Chinese Journal of Geochemistry 13(4), 371-378.
525
526

Captions of figures

Fig.1. Geological sketch map of the Jiangnan orogen, South China Craton (1: Jiangshan-Shaoxing fault; 2: Zhenghe-Dapu fault; 3: Northeast Jiangxi fault; 4: Jiujiang-Shitai fault; 5: Tanlu fault; SECCLMVZ: Southeast China costal late Mesozoic volcanic zone).

Fig.2. Geological sketch map of the Jiangshan-Shaoxing fault zone at Shijiao area, South China (Pt3sh: Shuangxiwu Group; Pt3h: Heshangzheng Group; Pt3z: Sinian System; Pt3ch: Chencai Complex).

Fig.3 Cross sections with sample locations.

Fig.4. Representative field photos of samples analyzed in this study. (A) Field photograph of the andesitic porphyrite sample 1468. (B) Field photograph showing the location of quartz diorite sample 1194. (C) Filed photograph of bedded chert. (D) Field photograph of the dunite within gabbro. (E) Field photograph of volcanic sedimentary rock sample 1470. (F) Field photograph showing the location of hornblende schist.

Fig.5. Photomicrographs of samples analyzed in this study. (A) Thin section

546 photomicrograph of amphibole pyroxenite sample 1472-11 (crossed nicols). (B) Thin
547 section photomicrograph of sample 1472-05 (crossed nicols). (C) Photomicrograph of
548 gabbro sample 1472-18 (crossed nicols). (D) Thin section photomicrograph of
549 amphibole pyroxenite sample 1472-11 (crossed nicols). (E) Photomicrograph of
550 quartz diorite sample 1194 (crossed nicols). (F) Photomicrograph of hornblende schist
551 (crossed nicols). Qz, quartz; Mus, Muscovite; Cpx, clinopyroxene; Ol, olivine; Plag,
552 plagioclase; HB, hornblende.

553

554 Fig.6. U–Pb concordia plots for zircons from quartz diorite and gabbro from the
555 Jiangshan-Shaoxing fault zone at Shijiao area, South China Craton.

556

557 Fig.7. A: Plot of εHf(t) vs. zircon U–Pb ages for the quartz diorite; B: Histogram of
558 zircon Hf model ages for the quartz diorite.

559

560 Fig.8. Zr/TiO2 vs Nb/Y diagram of analyzed mafic samples in this study.

561

562 Fig.9. (a), Chondrite-normalized REE patterns for analyzed samples (normalization
563 values are from Sun and McDonough (1989); (b) Primitive mantle-normalized
564 incompatible element distribution spider-grams for analyzed samples. The
565 normalization values are from McDonough and Sun (1995).

566

567 Fig.10. (a), Plot of Ti–Zr for gabbro samples (after Pearce, and Cann, 1973). (b),
568 Th–Hf–Ta diagram (after Wood, 1980) for the samples from Shijiao area (c), Plot of
569 Cr–Y for analyzed samples (after Mullen, 1983). (d) Plot of Rb–(Y+Nb) for quartz
570 diorite samples (after Pearce et al., 1984).

571

572 Fig. 11. Tectonic evolution model for the eastern Jiangshan-Shaoxing suture zone,
573 South China.

574

575 **Captions of tables**

576

577 Table 1 U-Pb data for zircons in gabbro and quartz diorite from the eastern
578 Jiangshan-Shaoxing fault zone at Shijiao, South China Craton.

579

580 Table 2 Hf isotope analyses for zircons in gabbro and quartz diorite from the eastern
581 Jiangshan-Shaoxing fault zone at Shijiao, South China Craton.

582

583 Table 3 Major and trace element data for representative samples from the eastern
584 Jiangshan-Shaoxing fault zone at Shijiao, South China Craton.

585

Table 1 U-Pb data for zircons in gabbro from the Shijiao area within the eastern Jiangshan-shaoxing fault zone

Analysis	CORRECTED RATIOS						CORRECTED AGES (Ma)						Th/U ratios	concor-dance
	207Pb/206Pb	1s	207Pb/235U	1s	206Pb/238U	1s	207Pb/206Pb	1s	207Pb/235U	1s	206Pb/238U	1s		
Sample 1194: Quartz diortie from the eastern Jiangshan-Shaoxing fault zone at Shijiao														
1155-01	0.060790	0.001700	1.253290	0.034040	0.149550	0.002290	632	62	825	15	898	13	1.06	109
1155-02	0.067630	0.001370	1.318450	0.025820	0.141410	0.002090	857	43	854	11	853	12	1.30	100
1155-03	0.067370	0.001140	1.314340	0.021600	0.141500	0.002020	849	36	852	9	853	11	0.86	100
1155-04	0.067330	0.001020	1.318810	0.019670	0.142070	0.001970	848	32	854	9	856	11	0.88	100
1155-05	0.067570	0.001420	1.319310	0.026870	0.141620	0.002100	855	45	854	12	854	12	0.97	100
1155-06	0.068270	0.001000	1.335020	0.019260	0.141850	0.001970	877	31	861	8	855	11	1.34	99
1155-07	0.067250	0.001310	1.317230	0.024680	0.142080	0.002080	846	41	853	11	856	12	0.90	100
1155-08	0.067510	0.002220	1.326200	0.041670	0.142480	0.002440	854	70	857	18	859	14	1.38	100
1155-09	0.067310	0.002390	1.314460	0.043980	0.141660	0.002700	847	76	852	19	854	15	1.01	100
1155-10	0.067300	0.001550	1.317440	0.029350	0.141990	0.002130	847	49	853	13	856	12	1.03	100
1155-11	0.067570	0.001730	1.321280	0.031940	0.141850	0.002270	855	54	855	14	855	13	1.07	100
1155-12	0.067520	0.001650	1.322180	0.030840	0.142050	0.002170	854	52	855	13	856	12	1.30	100
1155-13	0.067520	0.001770	1.318230	0.032750	0.141620	0.002270	854	56	854	14	854	13	1.15	100
1155-14	0.074230	0.005220	1.528950	0.102560	0.149430	0.004050	1048	146	942	41	898	23	1.38	95
1155-15	0.067560	0.001640	1.318900	0.030390	0.141620	0.002210	855	52	854	13	854	12	1.29	100
1155-16	0.067330	0.000770	1.315830	0.014990	0.141770	0.001860	848	24	853	7	855	11	1.06	100
1155-17	0.066590	0.001200	1.300060	0.022790	0.141630	0.001960	825	38	846	10	854	11	1.18	101
1155-18	0.067010	0.001740	1.304350	0.032420	0.141210	0.002210	838	55	848	14	852	12	1.20	100
1155-19	0.067000	0.001100	1.307450	0.020850	0.141570	0.001940	838	35	849	9	854	11	1.09	101
1155-20	0.067990	0.001700	1.322920	0.031580	0.141140	0.002190	868	53	856	14	851	12	0.93	99
Sample 1194-1: Quartz diorite from the eastern Jiangshan-Shaoxing fault zone at Shijiao														
1155-1-01	0.067740	0.001710	1.331980	0.031810	0.142640	0.002280	861	54	860	14	860	13	1.29	100
1155-1-02	0.067660	0.001280	1.325740	0.023930	0.142140	0.002070	858	40	857	10	857	12	1.40	100
1155-1-03	0.067520	0.001010	1.322110	0.019240	0.142050	0.001940	854	32	855	8	856	11	1.33	100
1155-1-04	0.067430	0.001500	1.312700	0.027610	0.141230	0.002180	851	47	851	12	852	12	1.05	100
1155-1-05	0.067750	0.001510	1.316370	0.028120	0.140950	0.002120	861	47	853	12	850	12	1.22	100
1155-1-06	0.068190	0.001180	1.325200	0.021910	0.140980	0.002020	874	37	857	10	850	11	1.38	99
1155-1-07	0.067260	0.001320	1.310610	0.024490	0.141350	0.002080	846	42	850	11	852	12	1.57	100
1155-1-08	0.067620	0.001160	1.320360	0.021990	0.141640	0.001960	857	36	855	10	854	11	1.11	100
1155-1-09	0.067360	0.001190	1.312410	0.022410	0.141330	0.001980	849	38	851	10	852	11	1.29	100
1155-1-10	0.067340	0.000950	1.313360	0.018020	0.141490	0.001920	848	30	852	8	853	11	1.53	100
1155-1-11	0.067710	0.000690	1.341040	0.014130	0.143670	0.001890	860	22	864	6	865	11	0.75	100
1155-1-12	0.067850	0.001870	1.344810	0.035900	0.143770	0.002240	864	59	865	16	866	13	0.96	100
1155-1-13	0.067850	0.001340	1.340490	0.025960	0.143300	0.002030	864	42	863	11	863	11	1.32	100
1155-1-14	0.069740	0.002290	1.351100	0.042490	0.140530	0.002390	921	69	868	18	848	14	1.29	98
1155-1-15	0.068650	0.002250	1.350820	0.042840	0.142740	0.002310	888	69	868	19	860	13	0.90	99
1155-1-16	0.067590	0.001670	1.337430	0.032260	0.143540	0.002130	856	53	862	14	865	12	1.03	100
1155-1-17	0.068210	0.001520	1.333790	0.029110	0.141840	0.002060	875	47	861	13	855	12	1.05	99
1155-1-18	0.067320	0.000900	1.331500	0.017900	0.143470	0.001920	848	28	860	8	864	11	1.20	100
1155-1-19	0.067800	0.001540	1.337150	0.029920	0.143060	0.002040	862	48	862	13	862	12	1.22	100
1155-1-20	0.067860	0.001560	1.336220	0.029890	0.142830	0.002080	864	49	862	13	861	12	0.94	100
Sample 1472: Gabbro from the eastern Jiangshan-Shaoxing fault zone at Shijiao														
1472-02	0.06821	0.0019	1.33354	0.03703	0.14182	0.00222	875	59	860	16	855	13	0.92	101
1472-03	0.06899	0.00127	1.43988	0.02782	0.15139	0.0021	898	39	906	12	909	12	0.97	100
1472-04	0.06841	0.00075	1.3402	0.01787	0.1421	0.00181	881	23	863	8	857	10	0.95	101
1472-05	0.07175	0.00346	1.50978	0.07018	0.15263	0.0032	979	101	934	28	916	18	0.66	102
1472-06	0.06887	0.0038	1.3581	0.07175	0.14303	0.00335	895	117	871	31	862	19	0.90	101
1472-07	0.06662	0.00138	1.30385	0.02801	0.14196	0.00199	826	44	847	12	856	11	3.39	99
1472-08	0.06763	0.00211	1.314	0.0404	0.14093	0.00231	857	66	852	18	850	13	0.83	100
1472-10	0.06976	0.00113	1.46442	0.02547	0.15228	0.00206	921	34	916	10	914	12	1.30	100
1472-11	0.06762	0.00076	1.30827	0.0177	0.14035	0.0018	857	24	849	8	847	10	1.34	100
1472-12	0.06795	0.00076	1.32689	0.01785	0.14165	0.00181	867	24	858	8	854	10	1.10	100
1472-16	0.06799	0.00171	1.34935	0.03423	0.14396	0.00216	868	53	867	15	867	12	1.23	100
1472-17	0.06779	0.00387	1.33085	0.07307	0.1424	0.00337	862	122	859	32	858	19	1.11	100
1472-18	0.06707	0.0021	1.33877	0.04135	0.14479	0.00239	840	67	863	18	872	13	1.62	99
1472-19	0.06734	0.00092	1.32629	0.02057	0.14286	0.00189	848	29	857	9	861	11	0.96	100
1472-20	0.06813	0.00133	1.33154	0.02717	0.14176	0.00201	873	41	860	12	855	11	0.92	101
1472-21	0.06778	0.00101	1.33643	0.02217	0.14301	0.00192	862	32	862	10	862	11	1.25	100
1472-22	0.06902	0.0017	1.34383	0.03337	0.14123	0.00215	899	52	865	14	852	12	0.91	102
1472-23	0.06899	0.00236	1.36084	0.04566	0.14308	0.0025	898	72	872	20	862	14	1.09	101
1472-24	0.06751	0.00398	1.32901	0.07533	0.14279	0.00345	854	126	858	33	860	19	0.92	100
1472-25	0.06781	0.00126	1.33105	0.02607	0.14238	0.00199	863	39	859	11	858	11	0.95	100
1472-26	0.0694	0.00198	1.36733	0.03906	0.14293	0.00234	911	60	875	17	861	13	1.10	102
1472-27	0.06972	0.00146	1.39221	0.03038	0.14487	0.00215	920	44	886	13	872	12	1.26	102
1472-28	0.06926	0.00143	1.37675	0.02982	0.1442	0.00213	906	44	879	13	868	12	0.99	101
1472-29	0.06846	0.00114	1.36304	0.02499	0.14443	0.00204	883	35	873	11	870	11	0.84	100
1472-30	0.06839	0.00231	1.36982	0.0456	0.14531	0.00256	880	72	876	20	875	14	1.17	100
1472-31	0.0686	0.00084	1.34523	0.01997	0.14226	0.00192	887	26	865	9	857	11	2.04	101
1472-32	0.06862	0.00177	1.34143	0.03508	0.14182	0.00223	887	55	864	15	855	13	1.14	101
1472-33	0.06984	0.00163	1.43484	0.03427	0.14905	0.00229	924	49	904	14	896	13	1.46	101

Table 2 Hf isotope analyses for zircons in gabbro and quartz diorite from the eastern Jiangshan-Shaoxing fault zone at Shijiao

Sample	176Yb/177	2σ	176Lu/177	2σ	176Hf/177	2σ	εHf(t)	εHf(0)	t	λ	T1 (Ma)	T2 (Ma)	fLu/Hf
Sample 1194: Quartz diorite from the eastern Jiangshan-Shaoxing fault zone at Shijiao													
1194-01	0.036205	0.000145	0.000608	0.000001	0.282555	0.00	11.80	-7.69	898	2.E-11	978	1027	-0.98
1194-02	0.066593	0.002380	0.001230	0.000061	0.282541	0.00	9.99	-8.16	853	2.E-11	1013	1107	-0.96
1194-03	0.022836	0.000061	0.000417	0.000002	0.282558	0.00	11.05	-7.56	853	2.E-11	968	1039	-0.99
1194-04	0.024684	0.000055	0.000440	0.000002	0.282552	0.00	10.89	-7.77	856	2.E-11	977	1052	-0.99
1194-05	0.033575	0.000232	0.000611	0.000003	0.282503	0.00	9.00	-9.52	854	2.E-11	1050	1171	-0.98
1194-06	0.051787	0.000209	0.000968	0.000001	0.282551	0.00	10.53	-7.81	855	2.E-11	992	1074	-0.97
1194-07	0.052784	0.000501	0.000916	0.000004	0.282537	0.00	10.08	-8.31	856	2.E-11	1010	1103	-0.97
1194-08	0.032453	0.000088	0.000580	0.000000	0.282518	0.00	9.65	-9.00	859	2.E-11	1028	1133	-0.98
1194-09	0.042549	0.000901	0.000742	0.000011	0.282487	0.00	8.35	-10.09	854	2.E-11	1076	1212	-0.98
1194-10	0.042784	0.000718	0.000707	0.000007	0.282540	0.00	10.29	-8.22	856	2.E-11	1001	1090	-0.98
1194-11	0.035768	0.000179	0.000604	0.000001	0.282573	0.00	11.51	-7.04	855	2.E-11	952	1012	-0.98
1194-12	0.031824	0.000308	0.000522	0.000007	0.282518	0.00	9.63	-8.99	856	2.E-11	1027	1132	-0.98
1194-13	0.038055	0.000454	0.000638	0.000004	0.282511	0.00	9.26	-9.25	854	2.E-11	1040	1154	-0.98
1194-14	0.029944	0.000285	0.000523	0.000002	0.282440	0.00	7.81	-11.72	898	2.E-11	1134	1280	-0.98
1194-15	0.041834	0.000441	0.000679	0.000011	0.282482	0.00	8.23	-10.25	854	2.E-11	1080	1219	-0.98
Sample 1194-1: Quartz diorite from the eastern Jiangshan-Shaoxing fault zone at Shijiao													
1194-1-01	0.042618	0.000163	0.000686	0.000004	0.282524	0.00	9.84	-8.77	860	2.E-11	1022	1122	-0.98
1194-1-02	0.047503	0.000541	0.000779	0.000005	0.282541	0.00	10.34	-8.15	857	2.E-11	1001	1088	-0.98
1194-1-03	0.019452	0.000152	0.000370	0.000002	0.282481	0.00	8.40	-10.30	856	2.E-11	1074	1210	-0.99
1194-1-04	0.053640	0.000269	0.000940	0.000005	0.282522	0.00	9.45	-8.84	852	2.E-11	1032	1140	-0.97
1194-1-05	0.032485	0.000313	0.000592	0.000007	0.282472	0.00	7.82	-10.62	850	2.E-11	1092	1242	-0.98
1194-1-06	0.029102	0.000163	0.000554	0.000003	0.282474	0.00	7.91	-10.55	850	2.E-11	1089	1236	-0.98
1194-1-07	0.030517	0.000140	0.000553	0.000004	0.282421	0.00	6.09	-12.41	852	2.E-11	1162	1353	-0.98
1194-1-08	0.032824	0.000095	0.000581	0.000003	0.282529	0.00	9.95	-8.58	854	2.E-11	1012	1110	-0.98
1194-1-09	0.028154	0.000201	0.000517	0.000007	0.282426	0.00	6.30	-12.22	852	2.E-11	1153	1340	-0.98
1194-1-10	0.033464	0.000298	0.000577	0.000002	0.282378	0.00	4.57	-13.94	853	2.E-11	1222	1450	-0.98
1194-1-11	0.043960	0.000459	0.000715	0.000004	0.282536	0.00	10.35	-8.35	865	2.E-11	1007	1093	-0.98
1194-1-12	0.050065	0.000190	0.000801	0.000002	0.282504	0.00	9.18	-9.49	866	2.E-11	1054	1168	-0.98
1194-1-13	0.057981	0.000315	0.000938	0.000001	0.282515	0.00	9.44	-9.09	863	2.E-11	1042	1149	-0.97
1194-1-14	0.055306	0.000232	0.000942	0.000001	0.282552	0.00	10.42	-7.78	848	2.E-11	990	1076	-0.97
1194-1-15	0.037050	0.000419	0.000660	0.000006	0.282539	0.00	10.39	-8.24	860	2.E-11	1001	1087	-0.98

Table 3 Major and trace element data for samples from the Shijiao area in the western Jiangnan orogenic belt

	1305	1305-1	1306-1	1306-1-1	1306-2	1306-2-1	1411	1402	1402-1	1405	1405-1	1405-2	1405-3	1407	1409	1414	1414-1	1414-2	1414-3
Major elements (wt%)																			
SiO2	56.43	55.78	55.23	54.72	4.48	4.51	6.71	47.84	47.20	47.51	48.69	51.03	51.07	70.06	67.59	49.68	49.77	49.32	49.89
TiO2	0.07	0.09	0.01	0.01	0.03	0.03	0.06	0.90	0.90	1.02	1.47	1.75	1.72	0.61	0.71	0.90	0.88	0.79	0.93
Al2O3	3.58	3.56	0.48	0.45	0.71	0.73	1.64	12.26	12.13	15.29	13.80	14.32	14.25	14.62	15.79	16.19	16.20	15.21	16.63
Fe2O3	1.23	1.34	0.27	0.27	3.37	3.37	0.60	10.67	10.68	8.89	9.94	10.90	10.87	4.15	5.45	10.04	10.04	10.51	10.04
MnO	0.00	0.00	0.01	0.01	0.13	0.13	0.04	0.14	0.14	0.12	0.15	0.16	0.16	0.11	0.12	0.19	0.19	0.14	0.21
MgO	31.45	31.42	30.51	30.30	20.90	20.74	19.26	13.31	13.28	7.77	6.50	7.04	6.96	1.44	1.75	8.61	8.64	8.86	8.41
CaO	0.17	0.23	3.46	3.43	28.03	27.92	28.76	8.49	8.42	7.08	7.81	6.02	5.97	1.04	0.59	6.39	6.42	8.17	4.82
Na2O	0.31	0.47	0.28	0.32	0.22	0.20	0.24	0.64	0.68	3.86	5.49	5.28	5.38	4.10	1.97	4.40	4.35	4.05	3.58
K2O	0.00	0.05	0.05	0.05	0.01	0.01	0.35	1.33	1.27	0.30	0.16	0.10	0.10	2.18	3.05	1.04	1.05	0.63	2.13
P2O5	0.02	0.03	0.15	0.15	0.03	0.03	0.08	0.18	0.20	0.10	0.16	0.13	0.14	0.14	0.14	0.12	0.12	0.09	0.09
LOI	6.43	6.34	9.57	9.56	42.94	42.93	43.09	4.72	4.64	9.00	6.64	2.61	2.55	2.13	3.01	3.22	3.00	2.76	2.95
TOTAL	99.69	99.23	99.95	99.22	100.85	100.61	100.90	100.80	100.00	101.10	101.00	99.34	99.17	100.70	100.40	101.10	101.10	100.70	99.67
Mg#	98	98	100	100	93	92	71	71	64	57	56	56	41	39	98	63	63	63	63
Trace elements (ppm)																			
Li	20.38	20.99	4.07	4.05	3.30	3.27	4.55	38.69	38.07	38.69	38.07	53.07	17.90	17.90	25.03	36.12	33.91	34.26	41.82
Be	0.24	0.31	0.24	0.20	0.11	0.12	0.74	0.70	0.67	0.70	0.67	0.72	1.02	1.52	1.84	0.71	0.29	0.73	0.88
Sc	2.65	2.96	1.76	1.85	1.79	1.71	1.04	16.16	17.82	16.16	17.82	27.08	33.08	9.62	12.96	29.47	25.59	31.15	34.39
Ti	603.2	554.9	275.7	269.6	109.7	88.24	87	5052	5036	5052	5036	5676	8296	3384	3923	5037	4443	5220	5986
V	27.98	25.75	12.44	13.04	6.82	6.36	0.71	214	221	214	221	106	185	42.62	52.16	122	111	126	258.5
Cr	35.89	21.59	14.97	15.34	11.15	8.46	11.87	630	627	630	627	282	168	46.32	72.65	282	363	287	299.2
Mn	41.06	31.34	1019	1055	89.43	82.32	237	1472	1462	1472	1462	1255	1558	1102	1303	2020	1538	2152	1631
Co	3.43	2.94	2.30	2.25	1.35	1.24	0.00	72.66	72.17	72.66	72.17	59.19	51.28	12.64	18.88	67.35	68.51	70.89	48.07
Ni	14.42	9.12	10.18	8.16	5.89	4.83	4.10	299	300	299	300	130	38.94	14.99	26.60	133	227	138	135.6
Cu	3.23	0.96	10.80	1.23	0.59	0.28	0.84	162	163	162	163	20.71	34.23	19.23	26.18	102	69.22	109	84.98
Zn	12.69	11.27	6.97	7.63	5.36	5.50	10.40	70.53	75.06	70.53	75.06	60.48	54.05	71.35	84.90	81.36	87.30	82.37	73.77
Ga	5.67	5.28	1.36	1.25	0.90	0.73	11.28	11.86	12.03	11.86	12.03	13.40	16.28	15.20	17.30	14.80	15.10	15.28	18.04
Rb	0.3	0.1	0.4	0.2	0.2	0.0	119.6	34.4	34.7	34.4	34.7	12.6	9.6	57.3	84.9	16.4	14.3	17.0	29.7
Sr	2.97	1.23	86.95	86.51	11.70	9.19	102	204	203	204	203	177	153	145	92.06	121	151	124	175.1
Y	1.01	0.81	3.70	3.67	1.12	1.05	0.56	16.26	16.40	16.26	16.40	19.54	26.12	32.73	31.61	22.30	14.55	23.12	19.08
Zr	30.47	29.94	12.79	13.05	5.73	4.63	4.92	96.07	95.98	96.07	95.98	70.26	111	226	215	83.65	67.76	88.70	104.1
Nb	1.67	1.56	0.96	0.81	0.34	0.21	0.72	9.91	9.90	9.91	9.90	3.37	5.11	11.40	13.45	4.55	2.34	3.62	3.62
Mo	0.23	0.06	0.60	0.64	0.07	0.10	0.09	0.50	0.47	0.50	0.47	0.10	0.12	0.28	0.23	0.22	0.18	0.19	0.24
Cd	0.05	0.07	0.07	0.07	0.04	0.05	-	-	-	-	-	-	-	-	-	-	-	-	0.22
Sn	0.82	0.36	0.21	0.19	0.11	0.10	1.35	1.79	1.75	1.79	1.75	1.33	0.54	1.63	2.33	0.98	0.92	1.54	1.04
Cs	0.50	0.41	0.14	0.11	0.67	0.69	2.57	0.88	0.90	0.88	0.90	2.43	11.18	4.82	5.60	1.75	2.52	1.79	3.85
Ba	3.11	0.84	9.88	5.64	1.22	0.76	471	468	463	468	463	129	56.41	635	467	285	202	330	825.6
La	4.56	4.52	2.79	2.26	0.46	0.34	1.44	15.09	14.81	15.09	14.81	6.75	8.20	26.79	29.96	11.70	5.16	12.03	9.49
Ce	9.36	9.14	6.39	5.60	1.26	0.98	2.37	30.12	26.99	30.12	26.99	18.42	22.73	54.55	60.29	27.35	14.09	28.08	21.60
Pr	0.88	0.88	0.79	0.68	0.17	0.14	0.30	3.18	3.12	3.18	3.12	2.00	2.55	6.85	7.38	2.63	1.52	2.66	2.65
Nd	2.82	2.86	3.22	2.74	0.79	0.63	0.92	13.43	13.14	13.43	13.14	9.57	12.42	27.09	28.91	11.46	7.25	11.69	11.10
Sm	0.34	0.33	0.73	0.63	0.22	0.18	0.18	2.83	2.79	2.83	2.79	2.56	3.30	5.12	5.49	2.72	1.87	2.77	2.68
Eu	0.04	0.04	0.22	0.19	0.06	0.05	0.69	0.98	0.95	0.98	0.95	1.05	1.06	1.31	1.28	0.86	0.72	0.88	0.98
Gd	0.23	0.21	0.67	0.64	0.24	0.23	0.18	2.76	2.73	2.76	2.73	2.64	3.36	4.84	5.28	2.83	1.97	2.89	3.09
Tb	0.03	0.02	0.09	0.09	0.03	0.03	0.03	0.45	0.44	0.45	0.44	0.49	0.63	0.78	0.86	0.51	0.36	0.51	0.44
Dy	0.17	0.16	0.66	0.61	0.20	0.20	0.20	2.55	2.53	2.55	2.53	2.94	3.86	4.52	5.07	3.18	2.22	3.21	3.15
Ho	0.04	0.04	0.13	0.13	0.04	0.04	0.04	0.47	0.47	0.47	0.47	0.55	0.73	0.91	1.00	0.63	0.42	0.64	0.71
Er	0.15	0.13	0.35	0.35	0.10	0.10	0.15	1.32	1.31	1.32	1.31	1.51	2.06	2.76	3.04	1.83	1.19	1.84	1.94
Tm	0.03	0.02	0.05	0.05	0.02	0.01	0.03	0.18	0.18	0.18	0.18	0.21	0.29	0.41	0.45	0.26	0.17	0.26	0.29
Yb	0.18	0.17	0.29	0.29	0.09	0.08	0.20	1.13	1.13	1.13	1.13	1.30	1.85	2.76	2.95	1.67	1.04	1.70	1.76
Lu	0.03	0.03	0.05	0.05	0.02	0.01	0.03	0.17	0.17	0.17	0.17	0.19	0.28	0.44	0.46	0.25	0.15	0.26	0.26
Hf	0.66	0.62	0.31	0.29	0.12	0.10	0.25	2.61	2.57	2.61	2.57	1.93	3.15	6.21	6.16	2.49	1.44	2.50	2.26
Ta	0.11	0.11	0.08	0.06	0.03	0.04	0.13	0.52	0.51	0.52	0.51	0.21	0.32	0.59	0.72	0.27	0.14	0.28	0.26
W	0.62	0.85	0.67	1.33	0.50	0.49	0.15	0.53	0.57	0.53	0.57	0.42	0.52	0.66	0.86	0.59	0.35	0.58	1.48
Pb	0.18	0.26	1.42	1.59	0.08	0.21	43.71	14.57	14.06	14.57	14.06	3.54	2.30	8.92	7.98	5.43	5.75	5.19	5.44
Bi	0.00	0.00	0.31	0.31	0.01	0.00	0.25	0.31	0.31	0.31	0.31	0.03	0.07	0.16	0.20	0.08	0.05	0.08	0.03
Th	1.54	1.55	0.69	0.72	0.20	0.19	0.00	2.29	2.64	2.29	2.64	1.14	2.35	7.99	10.24	2.84	0.56	2.87	2.88
U	0.81	0.80	0.57	0.59	0.28	0.28	0.20	0.51	0.55	0.51	0.55	0.34	0.59	1.23	1.58	0.33	0.14	0.33	0.45

Figure 1

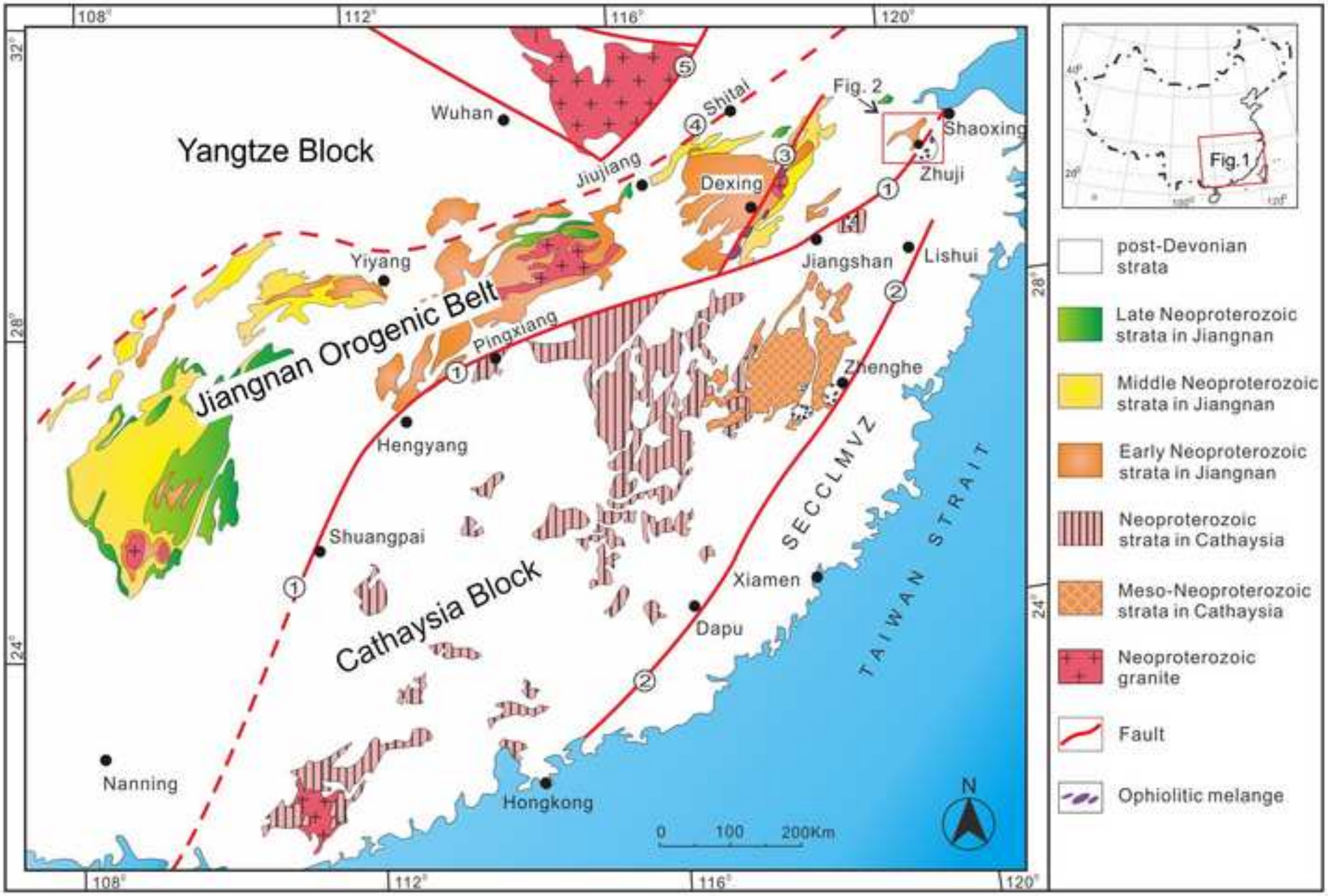
108°
112°
116°
120°
32°
28°
24°
Yangtze Block
Wuhan
Shitai
Jiujiang
Dexing
Fig. 2
Shaoxing
Zhuji
Yiyang
Jiangnan Orogenic Belt
Pingxiang
Jiangshan
Lishui
Zhenghe
Hengyang
Shuangpai
Cathaysia Block
SECCLMVZ
Xiamen
Dapu
TAIWAN STRAIT
Nanning
Hongkong
0 100 200Km
N
Fig. 1
post-Devonian strata
Late Neoproterozoic strata in Jiangnan
Middle Neoproterozoic strata in Jiangnan
Early Neoproterozoic strata in Jiangnan
Neoproterozoic strata in Cathaysia
Meso-Neoproterozoic strata in Cathaysia
Neoproterozoic granite
Fault
Ophiolitic melange

Figure 2

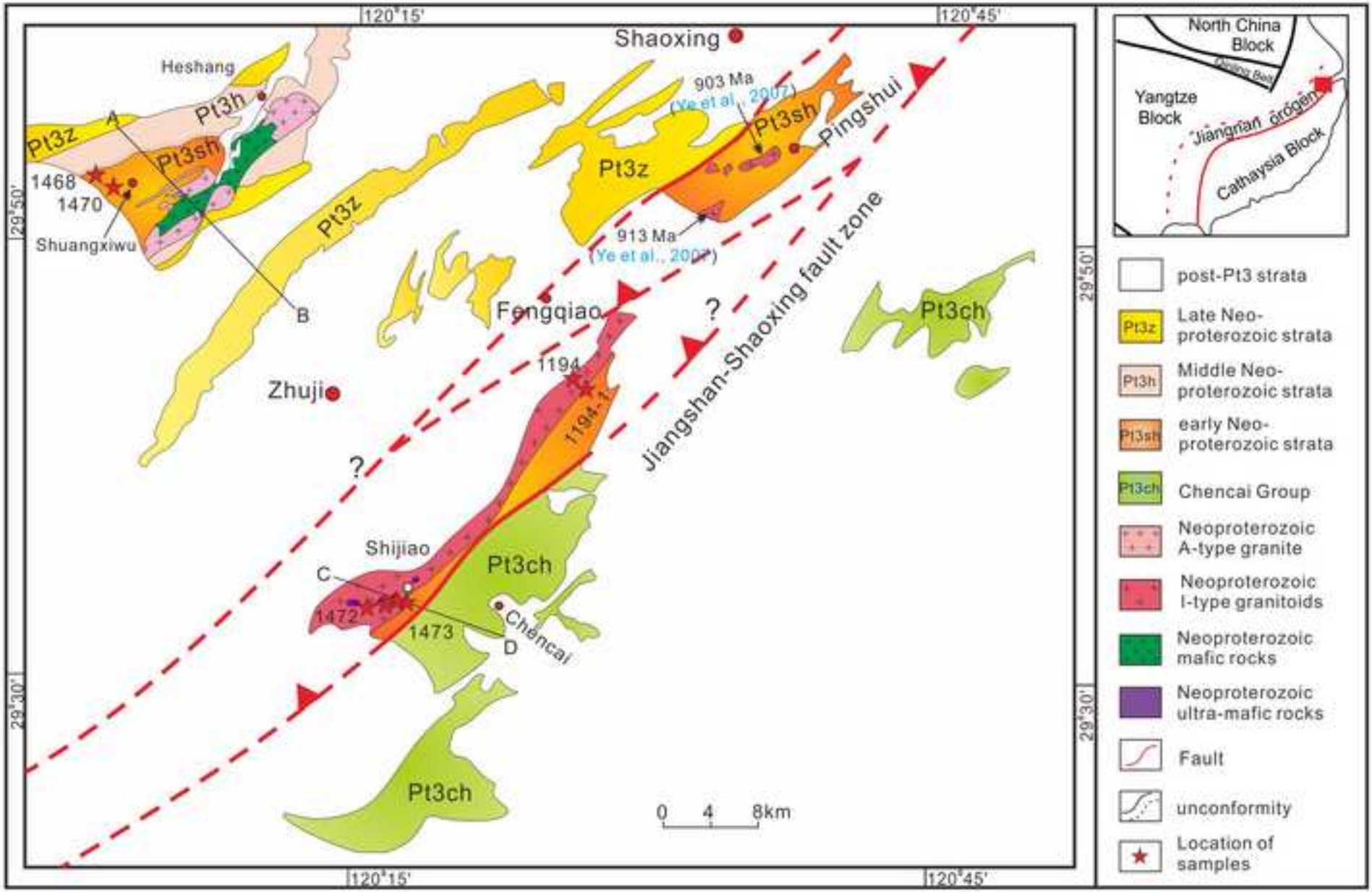
120°15'
120°45'
29°50'
29°30'
Shaoxing
Heshang
Pt3h
Pt3z
Pt3sh
1468
1470
Shuangxiwu
A
B
903 Ma
(Ye et al., 2007)
Pingshui
913 Ma
(Ye et al., 2007)
Fengqiao
Zhuji
1194
1194-1
Jiangshan-Shaoxing fault zone
?
Pt3ch
Shijiao
C
1472
1473
D
Chencai
0 4 8km
North China Block
Qinling Belt
Yangtze Block
Jiangnan orogen
Cathaysia Block
post-Pt3 strata
Late Neo-proterozoic strata
Middle Neo-proterozoic strata
early Neo-proterozoic strata
Chencai Group
Neoproterozoic A-type granite
Neoproterozoic I-type granitoids
Neoproterozoic mafic rocks
Neoproterozoic ultra-mafic rocks
Fault
unconformity
Location of samples

Figure 3

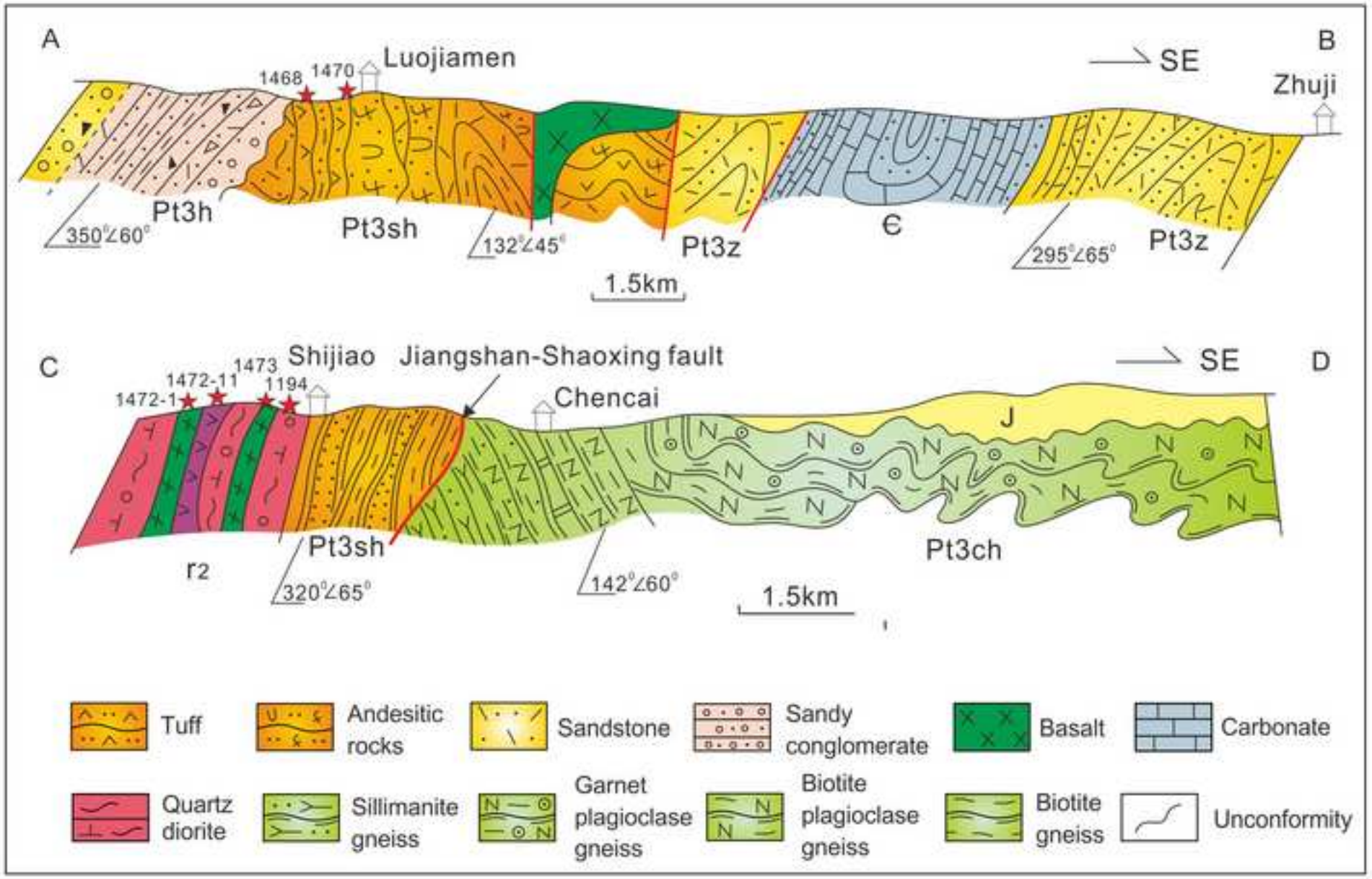
A
B
Luojiamen
1468
1470
SE
Zhuji
Pt3h
Pt3sh
Pt3z
Є
Pt3z
350°∠60°
132°∠45°
295°∠65°
1.5km
C
D
Shijiao
Jiangshan-Shaoxing fault
SE
1472-1
1472-11
1473
1194
Chencai
J
Pt3sh
Pt3ch
r2
320°∠65°
142°∠60°
1.5km
Tuff
Andesitic rocks
Sandstone
Sandy conglomerate
Basalt
Carbonate
Quartz diorite
Sillimanite gneiss
Garnet plagioclase gneiss
Biotite plagioclase gneiss
Biotite gneiss
Unconformity

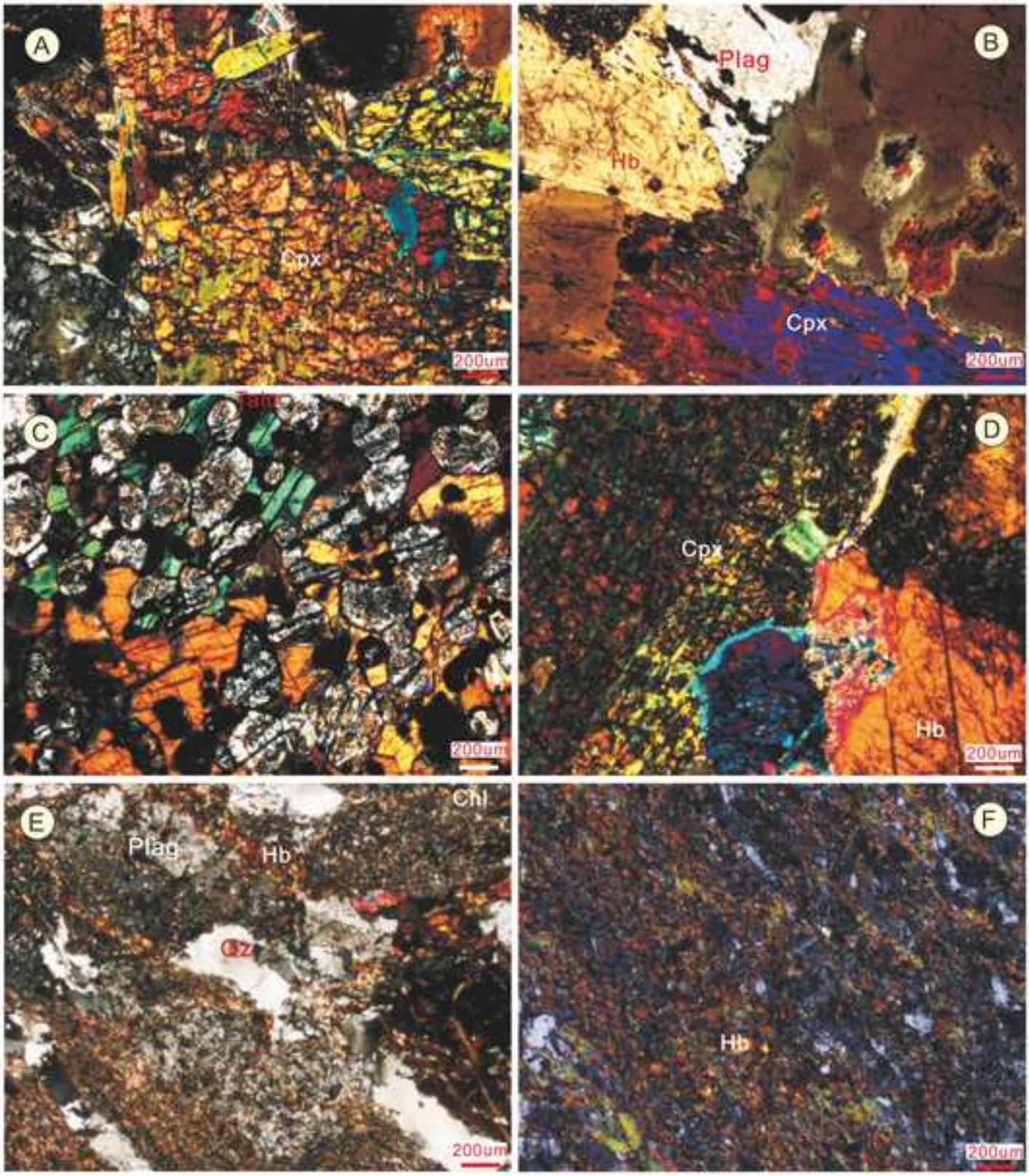

Figure 6

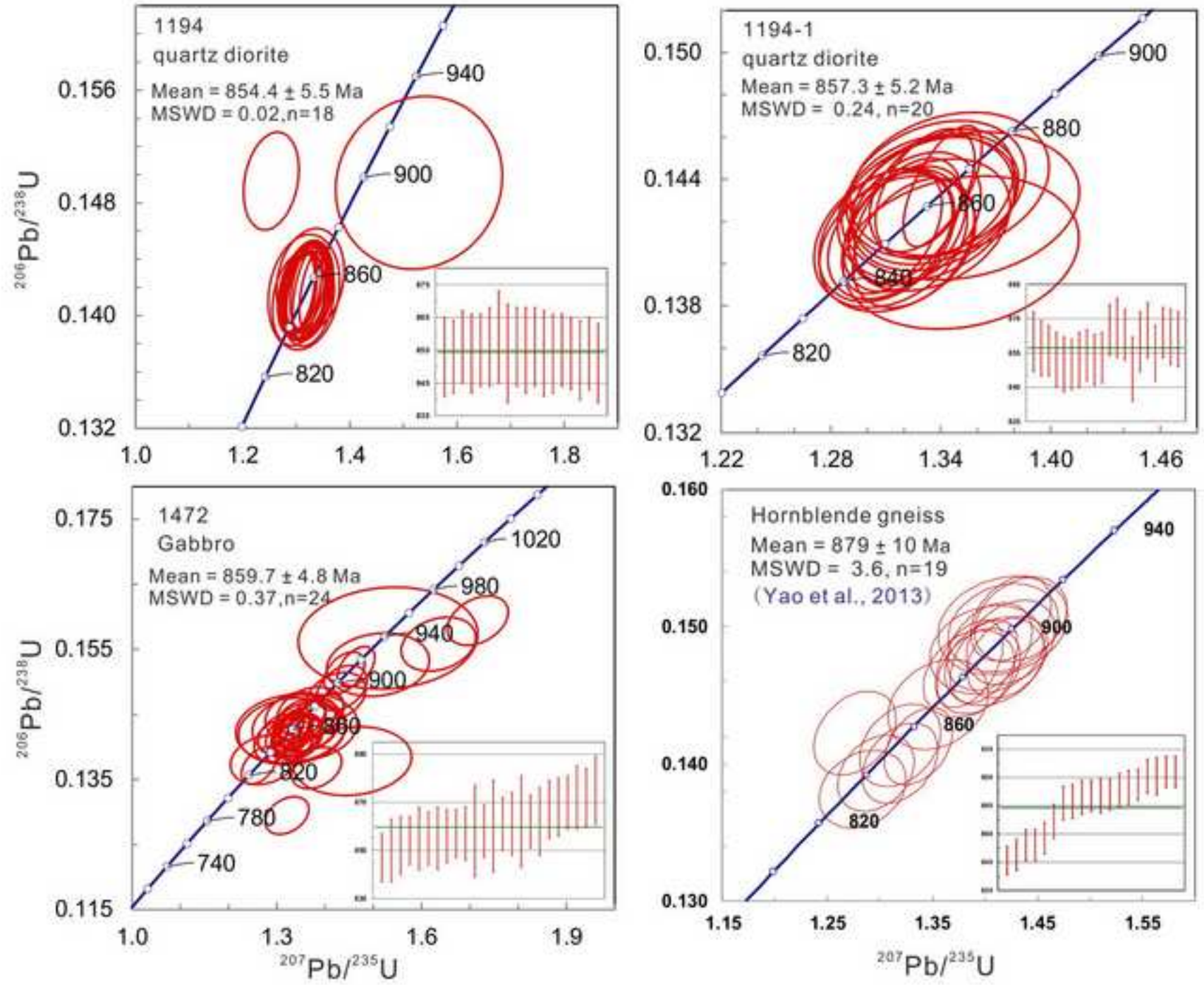
1194
quartz diorite
Mean = 854.4 ± 5.5 Ma
MSWD = 0.02,n=18
940
900
860
820
0.156
0.148
0.140
0.132
1.0
1.2
1.4
1.6
1.8
1194-1
quartz diorite
Mean = 857.3 ± 5.2 Ma
MSWD = 0.24, n=20
900
880
860
840
820
0.150
0.144
0.138
0.132
1.22
1.28
1.34
1.40
1.46
1472
Gabbro
Mean = 859.7 ± 4.8 Ma
MSWD = 0.37,n=24
1020
980
940
900
860
820
780
740
0.175
0.155
0.135
0.115
1.0
1.3
1.6
1.9
Hornblende gneiss
Mean = 879 ± 10 Ma
MSWD = 3.6, n=19
(Yao et al., 2013)
940
900
860
820
0.160
0.150
0.140
0.130
1.15
1.25
1.35
1.45
1.55
$^{206}Pb/^{238}U$
$^{207}Pb/^{235}U$

Figure 7

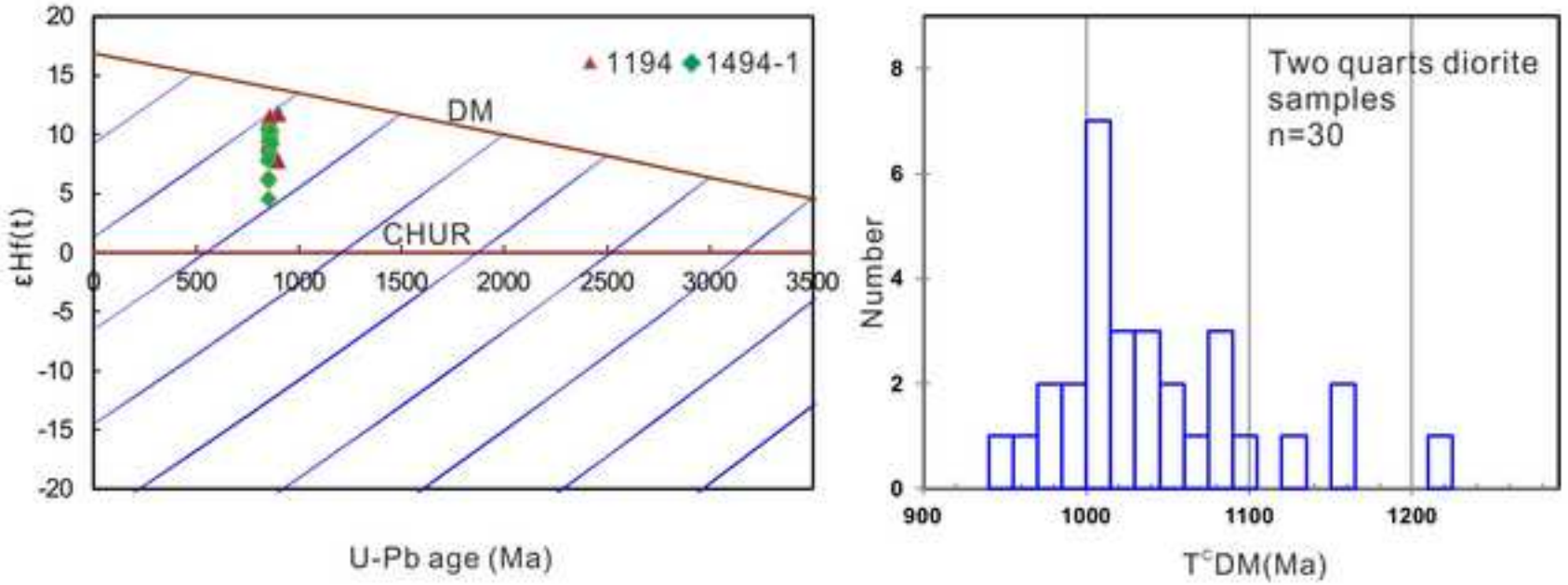

Figure 8

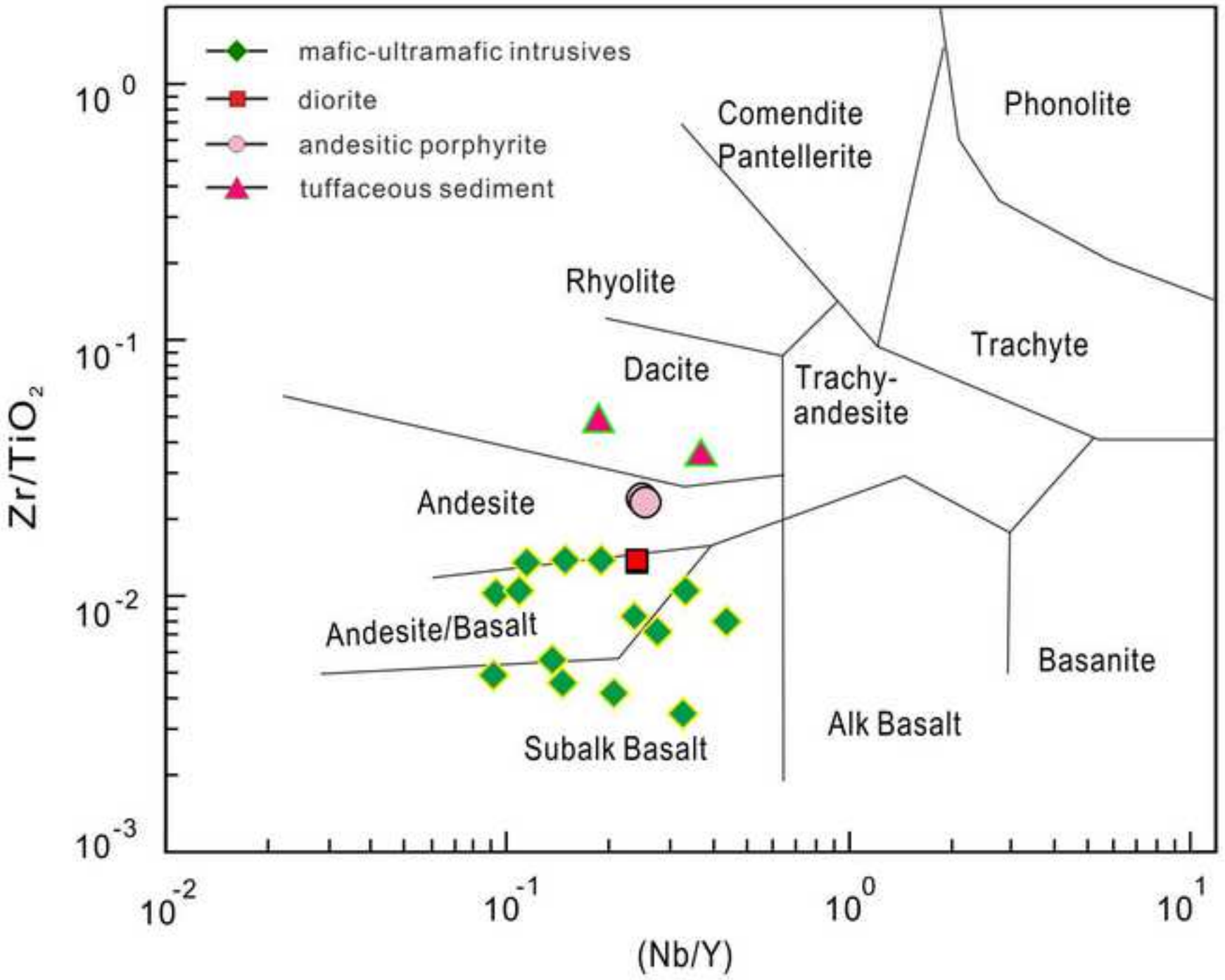
mafic-ultramafic intrusives
diorite
andesitic porphyrite
tuffaceous sediment
Comendite
Pantellerite
Phonolite
Rhyolite
Dacite
Trachyte
Trachy-
andesite
Andesite
Andesite/Basalt
Basanite
Alk Basalt
Subalk Basalt
10^{0}
10^{-1}
10^{-2}
10^{-3}
Zr/TiO_2
10^{-2}
10^{-1}
10^{0}
10^{1}
(Nb/Y)

Figure 9

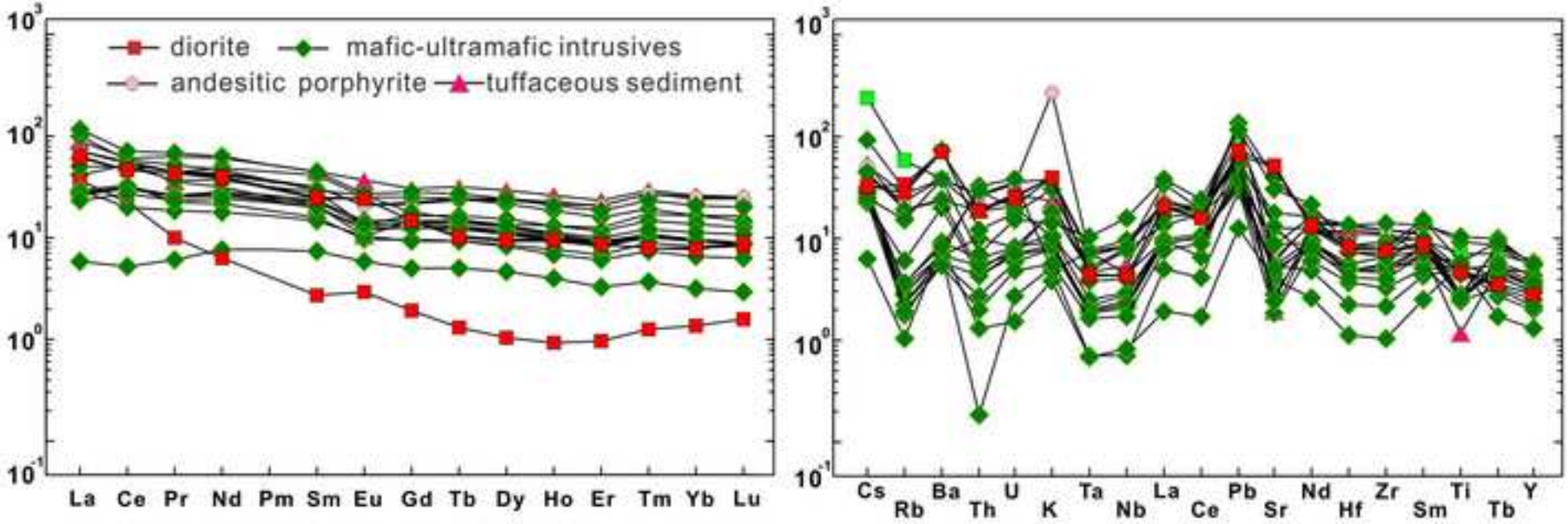

Figure 10

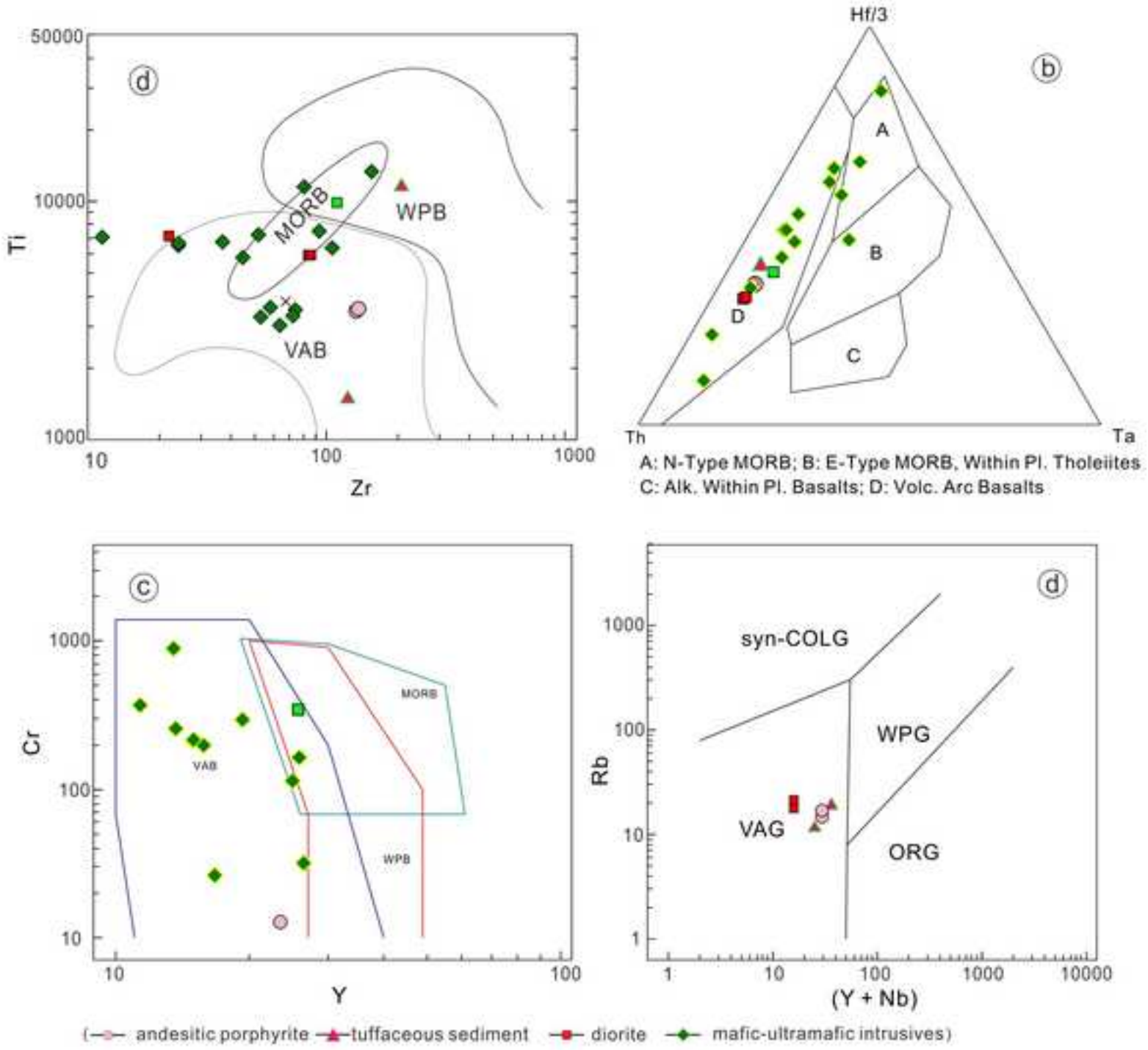
d
50000
10000
1000
Ti
10
100
1000
Zr
MORB
WPB
VAB
b
Hf/3
Th
Ta
A
B
C
D
A: N-Type MORB; B: E-Type MORB, Within Pl. Tholeiites
C: Alk. Within Pl. Basalts; D: Volc. Arc Basalts
c
1000
100
10
Cr
10
100
Y
MORB
VAB
WPB
d
1000
100
10
1
Rb
1
10
100
1000
10000
(Y + Nb)
syn-COLG
WPG
VAG
ORG
andesitic porphyrite
tuffaceous sediment
diorite
mafic-ultramafic intrusives

Figure 11

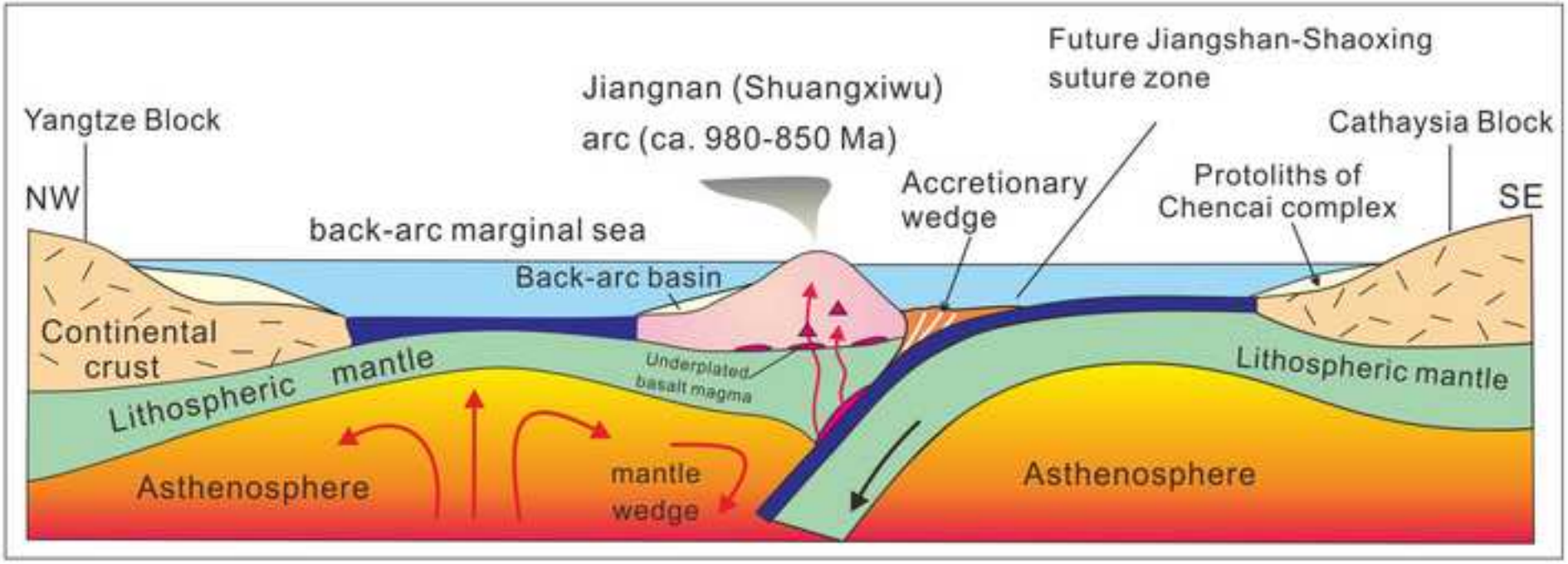
Future Jiangshan-Shaoxing
suture zone
Jiangnan (Shuangxiwu)
arc (ca. 980-850 Ma)
Yangtze Block
Cathaysia Block
NW
SE
Accretionary
wedge
Protoliths of
Chencai complex
back-arc marginal sea
Back-arc basin
Continental
crust
Lithospheric mantle
Underplated
basalt magma
Lithospheric mantle
Asthenosphere
mantle
wedge
Asthenosphere

Graphical Abstract (for review)